World Journal of Gastrointestinal Oncology

Submit a Manuscript: https://www.f6publishing.com

World J Gastrointest Oncol 2024 June 15; 16(6): 2697-2715

DOI: 10.4251/wjgo.v16.i6.2697

ISSN 1948-5204 (online)

ORIGINAL ARTICLE

Basic Study

Bidirectional effects of the tryptophan metabolite indole-3-acetaldehyde on colorectal cancer

Ze Dai, Kai-Li Deng, Xiao-Mei Wang, Dong-Xue Yang, Chun-Lan Tang, Yu-Ping Zhou

Specialty type: Oncology

Provenance and peer review: Unsolicited article; Externally peer reviewed.

Peer-review model: Single blind

Peer-review report's scientific quality classification

Grade A (Excellent): 0
Grade B (Very good): 0
Grade C (Good): C
Grade D (Fair): D
Grade E (Poor): 0

P-Reviewer: Fru PN, South Africa; Hashim Z, Pakistan

Received: December 17, 2023
Peer-review started: December 17, 2023
First decision: January 16, 2024
Revised: February 13, 2024
Accepted: March 25, 2024
Article in press: March 25, 2024
Published online: June 15, 2024

Ze Dai, Xiao-Mei Wang, Dong-Xue Yang, Yu-Ping Zhou, Department of Gastroenterology, The First Affiliated Hospital of Ningbo University, Ningbo 315020, Zhejiang Province, China

Ze Dai, Xiao-Mei Wang, Chun-Lan Tang, Health Science Center, Ningbo University, Ningbo 315211, Zhejiang Province, China

Kai-Li Deng, School of Traditional Chinese Medicine, Southern Medical University, Guangzhou 510515, Guangdong Province, China

Dong-Xue Yang, Yu-Ping Zhou, Institute of Digestive Disease of Ningbo University, Ningbo University, Ningbo 315020, Zhejiang Province, China

Dong-Xue Yang, Yu-Ping Zhou, Ningbo Key Laboratory of Translational Medicine Research on Gastroenterology and Hepatology, Ningbo Key Laboratory, Ningbo 315020, Zhejiang Province, China

Corresponding author: Yu-Ping Zhou, PhD, Doctor, Department of Gastroenterology, The First Affiliated Hospital of Ningbo University, No. 247 Renmin Road, Jiangbei District, Ningbo 315020, Zhejiang Province, China. fyzhouyuping@nbu.edu.cn

Abstract

BACKGROUND

Colorectal cancer (CRC) has a high incidence and mortality. Recent studies have shown that indole derivatives involved in gut microbiota metabolism can impact the tumorigenesis, progression, and metastasis of CRC.

AIM

To investigate the effect of indole-3-acetaldehyde (IAAD) on CRC.

METHODS

The effect of IAAD was evaluated in a syngeneic mouse model of CRC and CRC cell lines (HCT116 and DLD-1). Cell proliferation was assessed by Ki-67 fluorescence staining and cytotoxicity tests. Cell apoptosis was analysed by flow cytometry after staining with Annexin V-fluorescein isothiocyanate and propidium iodide. Invasiveness was investigated using the transwell assay. Western blotting and real-time fluorescence quantitative polymerase chain reaction were performed to evaluate the expression of epithelial-mesenchymal transition related genes and aryl hydrocarbon receptor (AhR) downstream genes. The PharmMap-

per, SEA, and SWISS databases were used to screen for potential target proteins of IAAD, and the core proteins were identified through the String database.

RESULTS

IAAD reduced tumorigenesis in a syngeneic mouse model. In CRC cell lines HCT116 and DLD1, IAAD exhibited cytotoxicity starting at 24 h of treatment, while it reduced Ki67 expression in the nucleus. The results of flow cytometry showed that IAAD induced apoptosis in HCT116 cells but had no effect on DLD1 cells, which may be related to the activation of AhR. IAAD can also increase the invasiveness and epithelial-mesenchymal transition of HCT116 and DLD1 cells. At low concentrations (< 12.5 μmol/L), IAAD only exhibited cytotoxic effects without promoting cell invasion. In addition, predictions based on online databases, protein-protein interaction analysis, and molecular docking showed that IAAD can bind to matrix metalloproteinase-9 (MMP9), angiotensin converting enzyme (ACE), poly(ADP-ribose) polymerase-1 (PARP1), matrix metalloproteinase-2 (MMP2), and myeloperoxidase (MPO).

CONCLUSION

Indole-3-aldehyde can induce cell apoptosis and inhibit cell proliferation to prevent the occurrence of CRC; however, at high concentrations (≥ 25 μmol/L), it can also promote epithelial-mesenchymal transition and invasion in CRC cells. IAAD activates AhR and directly binds MMP9, ACE, PARP1, MMP2, and MPO, which partly reveals why it has a bidirectional effect.

Key Words: Indole-3-acetaldehyde; Colorectal cancer; Tryptophan metabolism; Apoptosis; Epithelial-mesenchymal transition

Core Tip: In this study, we investigated the effect of an indole derivative of the gut microbiota, indole-3-acetaldehyde (IAAD), on colorectal cancer (CRC). The growth of tumors in a syngeneic mouse model, as well as the proliferation, apoptosis, invasion, and epithelial-mesenchymal transition of the HCT116 and DLD-1 cell lines, were observed. At low concentrations (< 12.5 μmol/L), IAAD can inhibit cell proliferation and induce cell apoptosis, but at high concentrations (≥ 25 μmol/L), it has a dual role of cytotoxicity and promotion of tumor cell invasiveness. Our results contribute to existing knowledge regarding the complex role of the gut microbiota in the occurrence and development of CRC.

Citation: Dai Z, Deng KL, Wang XM, Yang DX, Tang CL, Zhou YP. Bidirectional effects of the tryptophan metabolite indole-3-acetaldehyde on colorectal cancer. *World J Gastrointest Oncol* 2024; 16(6): 2697-2715
URL: https://www.wjgnet.com/1948-5204/full/v16/i6/2697.htm
DOI: https://dx.doi.org/10.4251/wjgo.v16.i6.2697

INTRODUCTION

Tumors are among the most important diseases threatening human health. In 2020, there were approximately 19.3 million new cancer cases and nearly 10 million cancer deaths worldwide. These conditions impose considerable burdens on human health and socioeconomic factors. Among these cases, colorectal cancer (CRC) ranks third in terms of the incidence of new tumors (10%) and is also the second leading cause of tumor-related deaths (9.4%)[1]. Although the prevalence of CRC has generally shown a decreasing trend in recent years, there has been a clear trend toward its resurgence. Unfortunately, the overall efficacy of advanced treatment is poor, and early diagnosis of CRC is challenging [2]. It has been established that a variety of factors, including genetic factors, smoking, and excessive alcohol intake, as well as red meat intake and weight gain, are involved in its development[3]. Recent studies revealed that the intestinal flora also plays a pivotal role in the carcinogenesis and progression of CRC[4].

The gut microbiota associated with CRC showed a decreased abundance of potentially protective taxa (*e.g.*, *Roseburia*) and an increased abundance of pro-oncogenic taxa (*e.g.*, *Bacteroides*, *Escherichia*, *Fusobacterium*, and *Porphyromonas*)[5-7]. These bacteria can act on tumors through related derived metabolites. For example, butyrate, which is a short-chain fatty acid, can downregulate proinflammatory cytokines[8], induce tumor cell apoptosis[9], and regulate intestinal regulatory T cells to improve the tumor immune microenvironment[10]. In addition, deoxycholic acid, which is a bile acid, has been demonstrated to have an *in vitro* effect of inducing oxidative damage to DNA[11], as well as a tumor-promoting effect [12].

Indole created during the metabolism of tryptophan (Trp) is also an important metabolite of the mammalian gut microbiota. In the colon, approximately 4%-6% of Trp is decomposed into indole[13]. From there, indole can be converted into indole-3-pyruvic acid, indole-3-acetaldehyde (IAAD)[14], indole acetic acid (IAA)[15], indole-3 aldehyde, 3- methylindole, the fecal odorant indole-3-lactic acid, indoleacrylic acid (ILA), and indole-3-propionic acid, among other molecules[14]. Several of these metabolic compounds have been shown to mediate antitumor effects[16-20], and their mechanism mainly involves direct effects on tumor cells and immune regulation. However, the role of many indole

derivatives has yet to be identified.

In this study, we evaluated the effect of IAAD, an unstudied intermediate in Trp metabolism, on CRC. The effects of IAAD on tumor proliferation, invasion, and apoptosis were evaluated *in vitro*. The results indicate that IAAD has a bidirectional effect. On the one hand, it can inhibit tumor cell proliferation and induce cell apoptosis; on the other hand, it promotes the invasiveness and epithelial-mesenchymal transition (EMT) of tumor cells.

MATERIALS AND METHODS

Animal modeling and intervention

BALB/c mice (male) were purchased from Jicui Pharmachem Biotechnology Co., Ltd. (Jiangsu, China) and then raised in a specific pathogen free barrier environment at the Experimental Animal Center of Ningbo University (Zhejiang, China). After one week of adaptive feeding, mice were inoculated with 2×10^6 CT-26 murine CRC cells in the posterior axilla to establish a syngeneic mouse model of CRC. The day after tumor implantation, mice in the IAAD treated group ($n = 5$) were given 200 μL of IAAD solution (40 mg/kg per mouse, dissolved in corn oil) by gavage once a day for 2 wk, and the control group ($n = 5$) was given the same volume of corn oil.

Cell culture and treatment

The human CRC cell lines DLD-1 and HCT116 were cultured in RPMI 1640 and McCoy's 5A medium (containing 10% fetal bovine serum and 1% penicillin/streptomycin), respectively, at 37 °C under 5% CO_2. While carrying out pharmacological intervention, the medium was changed to serum free medium. For better cell delivery, IAAD was dissolved in dimethyl sulfoxide (DMSO). The final concentration of DMSO was controlled at 0.1% in all the groups.

Cell viability assay

After treatment with different concentrations of IAAD, the culture media of the HCT116 and DLD-1 cells were aspirated. The culture wells were rinsed twice with phosphate buffered saline (PBS), 100 μL of basal medium and 10 μL of cell counting kit 8 solution (C6005, New Cell and Molecular Biotech, Suzhou, China) were added, and the plates were incubated for 2 h at 37 °C. The absorbance was measured at 450 nm by using a Multiskan SkyHigh full-wavelength microplate reader (A51119500C, Thermo Scientific™, United States). Cell viability was calculated as follows: [(As-Ab)/(Ac-Ab)] × 100%, where "As" is the absorbance of the drug-treated group, "Ac" is the absorbance of the control group, and "Ab" is the absorbance of the blank well.

Transwell invasion assay

Matrigel (356234, Corning, United States) was thawed at 4 °C and diluted with basal medium at a ratio of 1:8. One hundred microliters of diluted Matrigel was added to the transwell chambers (3422, Corning, United States) and incubated at 37 °C for 1 h to solidify. After the matrix was formed, the remaining liquid was removed, and 100 μL of basal medium was added for 30 min for hydration. In the lower chamber, 500 μL of complete medium (containing 20% fetal bovine serum) was added. Then, HCT116/DLD-1 cells (5×10^6 cells) treated with drugs or control cells were seeded into the upper chamber. After 48 h of culture, the cells that invaded the lower chamber were fixed with 4% paraformaldehyde and stained with crystal violet to evaluate the invasiveness of the cells.

Apoptosis detection

Annexin V-fluorescein isothiocyanate (Annexin V-FITC)/propidium iodide (PI) Apoptosis Kits were purchased from Elabscience (E-CK-A211, Wuhan, China). HCT116 and DLD-1 cells were digested with trypsin (0.25%, without ethylene diamine tetraacetic acid) and washed twice with PBS. Subsequently, Annexin V-FITC and PI were added to the cells resuspended in binding buffer for fluorescence staining. After incubating for 10 min in the dark, the fluorescence on cells was observed with a flow cytometer (CytoFlex S, BECKMAN, United States). The flow rate was controlled at approximately 500 cells/s, and the data from a total of 1.5×10^4 cells were collected. Finally, the exported Xit file was analyzed with FlowJo 10.8.1 software.

Immunofluorescence

HCT116 and DLD-1 cells were fixed with 4% paraformaldehyde, incubated with 0.2% Triton X-100, subjected to antigen retrieval with sodium citrate solution, and blocked with goat serum (B900780, Proteintech, United States). Then, the sections were incubated with primary antibodies [cadherin 2 (CDH2), 66219-1-lg Proteintech, United States; cadherin 1 (CDH1), 20874-1-AP, Proteintech, United States] and Ki-67-488 fluorescent labeled coupled antibodies (CL488-27309, Proteintech, United States) overnight at 4 °C. The next day, after washing three times with PBS-T (0.2%), the sections were incubated with fluorescently labeled secondary antibodies (SA00013-2, SA00013-3, Proteintech, United States) corresponding to the species for 2 h at room temperature. Finally, the nuclei were stained with DAPI (C0060, Solarbio, Beijing, China) and imaged under a confocal microscope (TCS SP8 X, Leica, German).

Western blot analysis

Total proteins were extracted from HCT116 and DLD-1 cells using RIPA lysis buffer (WB310, NCM Biotech, Suzhou, China). The protein homogenate from the previous step was supplemented with 5 × loading buffer (WB2001, NCM Biotech, Suzhou, China) and then heated at 95 °C for 5 min to denature the proteins. The electrophoresis conditions

included the following parameters: 80 V for 30 min and a switch to 120 V for 60 min. The membrane transfer conditions involved 400 mA for 90 min. Moreover, skim milk was used for blocking at room temperature for 2 h, after which primary antibodies were added to the sample. Antibodies (CDH2, 66219-1-lg, Proteintech, United States; CDH1, 20874-1-AP, Proteintech, United States) were incubated overnight at 4 °C. On the following day, the polyvinylidene fluoride membrane with adsorbed proteins was washed three times with TBS-T (0.1%) for 10 min each time, followed by incubation at room temperature with HRP-coupled secondary antibodies [anti-rabbit IgG, HRP-linked antibody, 7074, Cell Signaling Technology, United States; goat anti-mouse IgG (H + L) HRP, S0002, Affinity, United States]. The membrane was washed again with TBS-T (0.1%). Finally, the bands were visualized in an ultrasensitive chemiluminescence system (5300 M, TANAN, Shanghai, China).

Real-time fluorescence quantitative polymerase chain reaction

Total intracellular mRNA in HCT116 and DLD-1 cells was extracted by using a Sparkjade Cellular RNA Extraction Kit (AC0205, Shandong, China), followed by reverse transcription and real-time fluorescence quantification by using RT mix (R2020L United States Everbright® Inc, Suzhou, China) and SYBR Green qPCR Supermix (S2024L, Everbright® Inc, Suzhou, China), respectively. Real-time fluorescence quantification was performed on a Technology Fluorescence Quantitative Polymerase Chain Reaction Detection System (FQD-96A, Bioer, Hangzhou, China), and the amplification program was set to 95 °C for 120 s, followed by 45 extension cycles (95 °C, 5 s; 60 °C, 30 s). The sequences of primers used are shown in Table 1.

Prediction of targets of IAAD therapy in CRC

The PubChem database (https://pubchem.ncbi.nlm.nih.gov) was used to obtain standard SMILES and 3D structures of IAAD sequences, which were further imported into the PharmMapper database (http://www.lilab-ecust.cn/pharmmapper), SEA database (https://sea.bkslab.org), and SWISS database (http://www.swisstargetprediction.ch) to predict targets. The term "CRC" was used as a keyword in the GeneCards database (https://www.genecards.org) to retrieve the disease-related genes linked to CRC with a relevance score > 1. The CRC gene set and IAAD gene set were intersected to obtain the common targets.

Protein functional enrichment analysis

Gene Ontology (GO) and Kyoto Encyclopedia of Genes and Genomes (KEGG) enrichment analyses were performed with the DAVID database (https://david.ncifcrf.gov/). Potential targets of IAAD in the treatment of CRC were imported into the String database (https://string-db.org), and the species was defined as "*Homo sapiens*" to construct the protein-protein interaction (PPI) network. PPI networks were analyzed with Cytoscape 3.9.1 and its cytoHubba and MCODE plug-ins.

Molecular docking

IAAD was molecularly docked with the core target. The 3D structure of the protein corresponding to the key target gene was downloaded from the PDB database (http://www.rcsb.org/), and molecular docking was performed by using AutoDock Vina visual analysis software. The docking possibility was evaluated by the spatial sites and binding energy after docking.

Statistical analysis

All data are shown as the mean ± SD. The Shapiro-wilk test was used to verify the normal distribution. Student's *t* test or one-way analysis of variance (ANOVA) were employed to decide significant differences between two or multiple groups where appropriate. *F* test and Brown-Forsythe test were further used to verify the homogeneity of variance, and Student's *t* test with Welch's correction and Welch's ANOVA were used when necessary. For measurement data that didnot conform to a normal distribution, Mann-Whitney test or Kruskal-Wallis test was employed to decide significant differences between two or multiple groups. Dunn's multiple comparisons test was used to further calibrate the *P* value. All calculations were conducted with GraphPad Prism (La Jolla, CA, United States). A *P* value of 0.05 or lower was considered significant.

RESULTS

IAAD inhibits tumor growth in vivo

To determine the role of IAAD in CRC, a syngeneic mouse model of CRC was generated by subcutaneous implantation of CT26 (a mouse-derived CRC cell line). The experimental design is shown in Figure 1A (n = 5). There was no significant difference in mouse weight change between the IAAD treatment group and the control group, and no mice died during the experimental period (Figure 1B). Tumor nodules were palpable in the posterior axilla 6 d after subcutaneous inoculation of CT26 cells. Compared with the control group, the IAAD intervention group had a slower rate of volume increase ($P < 0.05$) (Figure 1B). The volume (566.80 g ± 169.60 g *vs* 1096.00 g ± 352.70 g, $P = 0.0165$) and weight (0.84 g ± 0.24 g *vs* 1.24 g ± 0.23 g, $P = 0.0277$) of the tumors in the IAAD treatment group were significantly lower than those of the control group (Figure 1C-E). These findings suggest that IAAD could inhibit the colonization and growth of CRC cells.

Table 1 List of primers

Gene	Primer sequence	
	Forward (5' to 3')	Reverse (5' to 3')
VIM	GACGCCATCAACACCGAGTT	CTTTGTCGTTGGTTAGCTGGT
SNAI1	TCGGAAGCCTAACTACAGCGA	AGATGAGCATTGGCAGCGAG
OCLN	ACAAGCGGTTTTATCCAGAGTC	GTCATCCACAGGCGAAGTTAAT
CDH1	CGAGAGCTACACGTTCACGG	GGGTGTCGAGGGAAAAATAGG
CDH2	TCAGGCGTCTGTAGAGGCTT	ATGCACATCCTTCGATAAGACTG
CYP1A1	TCGGCCACGGAGTTTCTTC	GGTCAGCATGTGCCCAATCA
CYP1B1	TGAGTGCCGTGTGTTTCGG	GTTGCTGAAGTTGCGGTTGAG

VIM: Vimentin; *SNAI1*: Snail family transcriptional repressor 1; *OCLN*: Occludin; *CDH1*: Cadherin 1; *CDH2*: Cadherin 2; *CYP1A1*: Cytochrome P450 family 1 subfamily A member 1; *CYP1B1*: Cytochrome P450 family 1 subfamily B member 1.

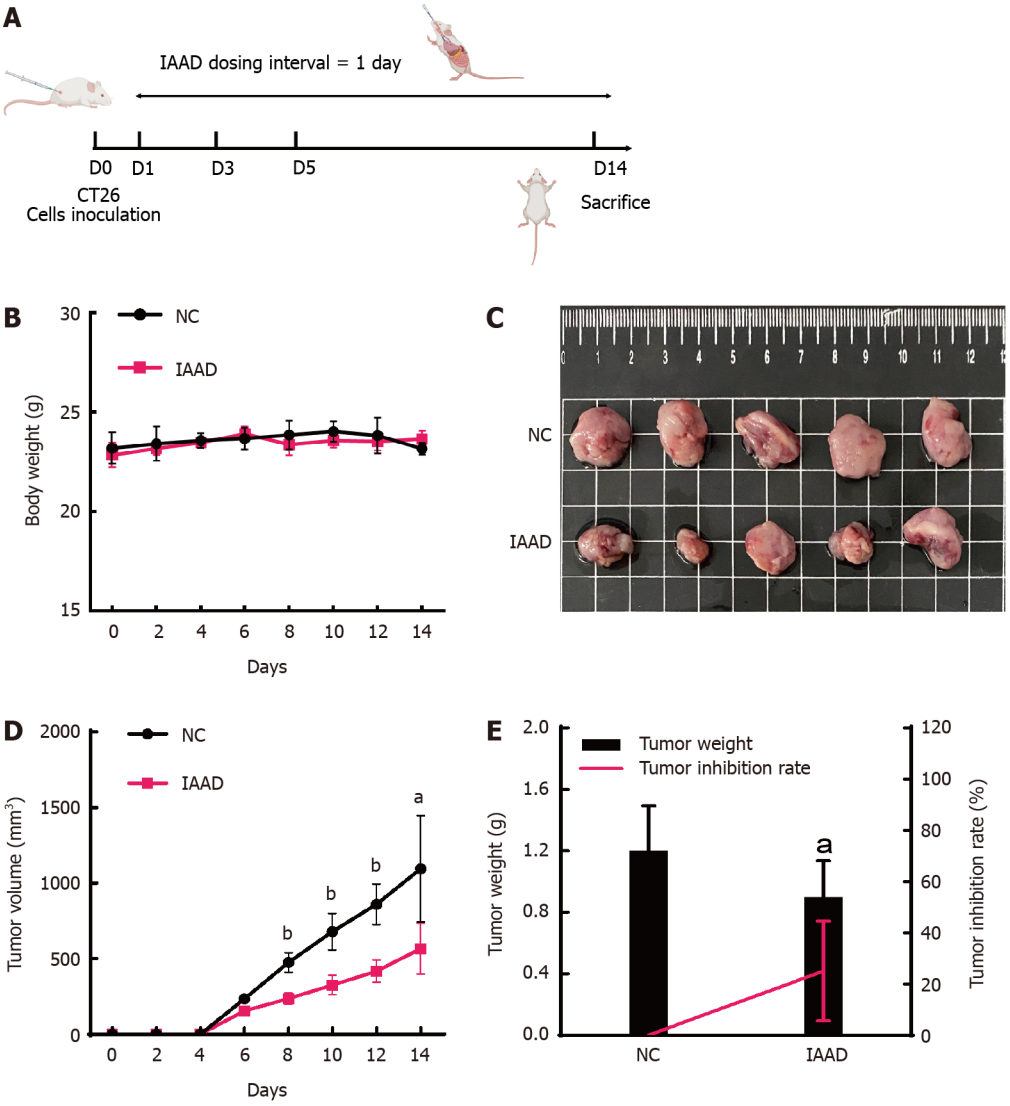

Figure 1 Anti-tumor effect of indole-3-acetaldehyde *in vivo*. A: Flowchart of the experiment; B: Changes in body weight; C: Macroscopic view of the subcutaneous tumor; D: Changes in tumor volume; E: Subcutaneous tumor weight and tumor inhibition rate. [a]*P* < 0.05 *vs* control group; [b]*P* < 0.01 *vs* control group. IAAD: Group of mice receiving indole-3-acetaldehyde (dissolved in corn oil); NC: Group of mice receiving corn oil.

IAAD inhibits proliferation and induce apoptosis of CRC cells in vitro

IAAD can be metabolized *in vivo* to other indole derivatives, which have been proven to inhibit CRC[16]. To rule out this possibility, further experiments were performed with the human colorectal carcinoma cell lines HCT116 and DLD-1. The results of the cytotoxicity tests suggested that IAAD at high doses (50 μmol/L and 100 μmol/L) had an inhibitory effect on cell proliferation after 24 h of treatment (Figure 2A and B). After being treated with different concentrations of IAAD for 48 h, the viability of HCT116 (82.82% ± 4.06% *vs* 100.00% ± 4.39%, 100 μmol/L, $P < 0.001$) and DLD-1 (78.66% ± 7.68% *vs* 101.50% ± 5.88%, 100 μmol/L, $P < 0.001$) cells significantly decreased compared with the control group (Figure 2C and D), and it is worth noting that the inhibitory effect became more pronounced with increasing concentration. Direct immunofluorescence staining demonstrated that IAAD intervention dose-dependently induced a decrease of Ki-67 expression in the nuclei of HCT116 and DLD-1 cells (Figure 2E and F). These findings suggest that IAAD inhibits CRC cell proliferation *in vitro*.

Moreover, flow cytometry results revealed that the proportions of total apoptotic cells (50 μmol/L: 19.08% ± 2.17% *vs* 4.38% ± 1.02%, $P < 0.001$; 100 μmol/L: 24.63% ± 0.75% *vs* 4.38% ± 1.02%, $P < 0.001$) were significantly increased in HCT116 cells treated with IAAD (Figure 3A and B), but no similar effect was observed in DLD-1 cells (50 μmol/L: 0.23% ± 0.04% *vs* 0.26% ± 0.05%, $P = 0.5934$; 100 μmol/L: 0.18% ± 0.09% *vs* 0.26% ± 0.05%, $P > 0.999$) (Figure 3C and D). Various indole derivatives exert their functions on tumor cells by activating the aryl hydrocarbon receptor (AhR)[18,21]. Cytochrome P450 family 1 subfamily A member 1 (*CYP1A1*) and cytochrome P450 family 1 subfamily B member 1 (*CYP1B1*) are downstream target genes of the AhR signaling pathway and can prompt its activation. After treatment with IAAD for 48 h, the mRNA abundance (fold change) of *CYP1A1* (50 μmol/L: 2.297 ± 0.315 *vs* 1.000 ± 0.104, $P = 0.0021$; 100 μmol/L: 2.331 ± 0.338 *vs* 1.000 ± 0.104, $P = 0.0018$) and *CYP1B1* (50 μmol/L: 3.553 ± 0.475 *vs* 1.000 ± 0.092, $P < 0.001$; 100 μmol/L: 4.207 ± 0.612 *vs* 1.000 ± 0.092, $P < 0.001$) in HCT116 cells significantly increased compared to the control group (Figure 3E). Meanwhile, although the mRNA expression levels of *CYP1A1* (50 μmol/L: 1.226 ± 0.153 *vs* 1.000 ± 0.036, $P = 0.0542$; 100 μmol/L: 1.583 ± 0.126 *vs* 1.000 ± 0.036, $P = 0.0015$) and *CYP1B1* (50 μmol/L: 1.727 ± 0.203 *vs* 1.000 ± 0.098, $P = 0.0080$; 100 μmol/L: 1.889 ± 0.266 *vs* 1.000 ± 0.098, $P = 0.003$) in DLD-1 have also increased (Figure 3F), the magnitude of the increase was relatively small. This may be the reason why the proportion of apoptosis in DLD-1 cells remained unchanged. These results suggest that IAAD, like other indole derivatives, may induce cytotoxicity in cancer cells *via* activation of AhR.

IAAD promotes invasiveness and EMT of CRC cells in vitro

The effect of IAAD on the invasiveness of CRC cell lines was evaluated by a transwell assay. After 48 h of treatment with IAAD, the number of HCT116 (50 μmol/L: 130.80 ± 32.90 *vs* 36.25 ± 14.06, $P = 0.0039$; 100 μmol/L: 253.50 ± 21.76 *vs* 36.25 ± 14.06, $P < 0.001$) and DLD-1 (50 μmol/L: 163.00 ± 13.44 *vs* 70.50 ± 15.50, $P < 0.001$; 100 μmol/L: 230.00 ± 49.16 *vs* 70.50 ± 15.50, $P = 0.0063$) cells with the ability to penetrate the matrix gel significantly increased compared to the control group (Figure 4A and B).

Changes in tumor invasiveness are related to the process of EMT[22]. The mRNA expression levels of EMT-related genes including *CDH1*, *CDH2*, vimentin (*VIM*), occludin (*OCLN*), and snail family transcriptional repressor 1 (*SNAI1*) were determined. In the DLD1 cell line, the mRNA expression levels (fold change) of *OCLN* (50 μmol/L: 0.600 ± 0.004 *vs* 1.000 ± 0.012, $P < 0.001$; 100 μmol/L: 0.423 ± 0.010 *vs* 1.000 ± 0.012, $P < 0.001$) and *SNAI1* (50 μmol/L: 0.760 ± 0.066 *vs* 1.000 ± 0.077, $P = 0.0115$; 100 μmol/L: 0.639 ± 0.074 *vs* 1.000 ± 0.077, $P = 0.0016$) were downregulated, while the mRNA expression of *VIM* (50 μmol/L: 1.360 ± 0.284 *vs* 1.000 ± 0.217, $P = 0.1931$; 100 μmol/L: 1.583 ± 0.175 *vs* 1.000 ± 0.217, $P = 0.0406$) was increased. In contrast, the mRNA expression levels of *SNAI1* (50 μmol/L: 0.883 ± 0.105 *vs* 1.000 ± 0.129, $P = 0.3324$; 100 μmol/L: 0.902 ± 0.081 *vs* 1.000 ± 0.129, $P = 0.4323$) and *CDH1* (50 μmol/L: 0.846 ± 0.258 *vs* 1.000 ± 0.205, $P = 0.563$; 100 μmol/L: 0.731 ± 0.169 *vs* 1.000 ± 0.205, $P = 0.2573$) were decreased, while that of *CDH2* (50 μmol/L: 2.481 ± 0.845 *vs* 1.000 ± 0.049, $P = 0.3594$; 100 μmol/L: 4.006 ± 0.728 *vs* 1.000 ± 0.049, $P = 0.0146$) was increased in the HCT116 cells (Figure 4C). In addition, immunofluorescence and Western blot analysis showed an increase in protein expression levels of CDH2 in both HCT116 and DLD-1 cells, whereas the protein expression level of CDH1 decreased in HCT116 cells, but did not show significant changes in DLD-1 cells (Figure 4D and E). The abovementioned results suggest that IAAD promotes EMT in CRC cell lines.

Low concentrations of cytotoxic IAAD does not promote tumor cell invasion

At high concentrations (≥ 50 μmol/L), the cytotoxicity, EMT induction, and pro-invasive effects of IAAD in CRC are positively correlated with its concentrations. However, it is not yet clear whether the bidirectional effects still exist at low concentrations. Therefore, we preliminarily observed the effect of IAAD on CRC at low concentrations based on cell viability and the mRNA expression level of *CDH2*. Among the two CRC cell lines, we chose the HCT116 cell line for subsequent experiments because of its favorable phenotype. When the concentration of IAAD was lower than 12.5 μmol/L, there was no significant difference in the mRNA expression level (fold change) of *CDH2* (12.5 μmol/L: 1.175 ± 0.296 *vs* 1.000 ± 0.305, $P = 0.9968$; 25 μmol/L: 1.798 ± 0.684 *vs* 1.000 ± 0.305, $P = 0.2980$; 50 μmol/L: 2.792 ± 0.614 *vs* 1.000 ± 0.305 $P = 0.0030$) (Figure 5A), but the cytotoxicity of IAAD in this concentration range still existed (Figure 1C). Further experiments also revealed that HCT116 cells were induced to undergo apoptosis (12.5 μmol/L: 18.940% ± 2.282% *vs* 9.277% ± 0.313%, $P = 0.0031$; 25 μmol/L: 23.13% ± 3.037% *vs* 9.277% ± 0.313%, $P < 0.001$) and inhibited from proliferation under IAAD at 12.5 μmol/L (Figure 5B-D). Moreover, the invasiveness of HCT116 cells did not change under treatment with IAAD at 12.5 μmol/L (26.75 ± 4.922 *vs* 22.00 ± 3.651, $P = 0.3166$), but increased under treatment with IAAD at 25 μmol/L (63.00 ± 18.87 *vs* 22.00 ± 3.651, $P = 0.0309$) (Figure 5E and F).

Network analysis of proteins that can be directly bound by IAAD

A total of 99 common targets of IAAD were obtained. GO and KEGG analyses were performed based on the abovemen-

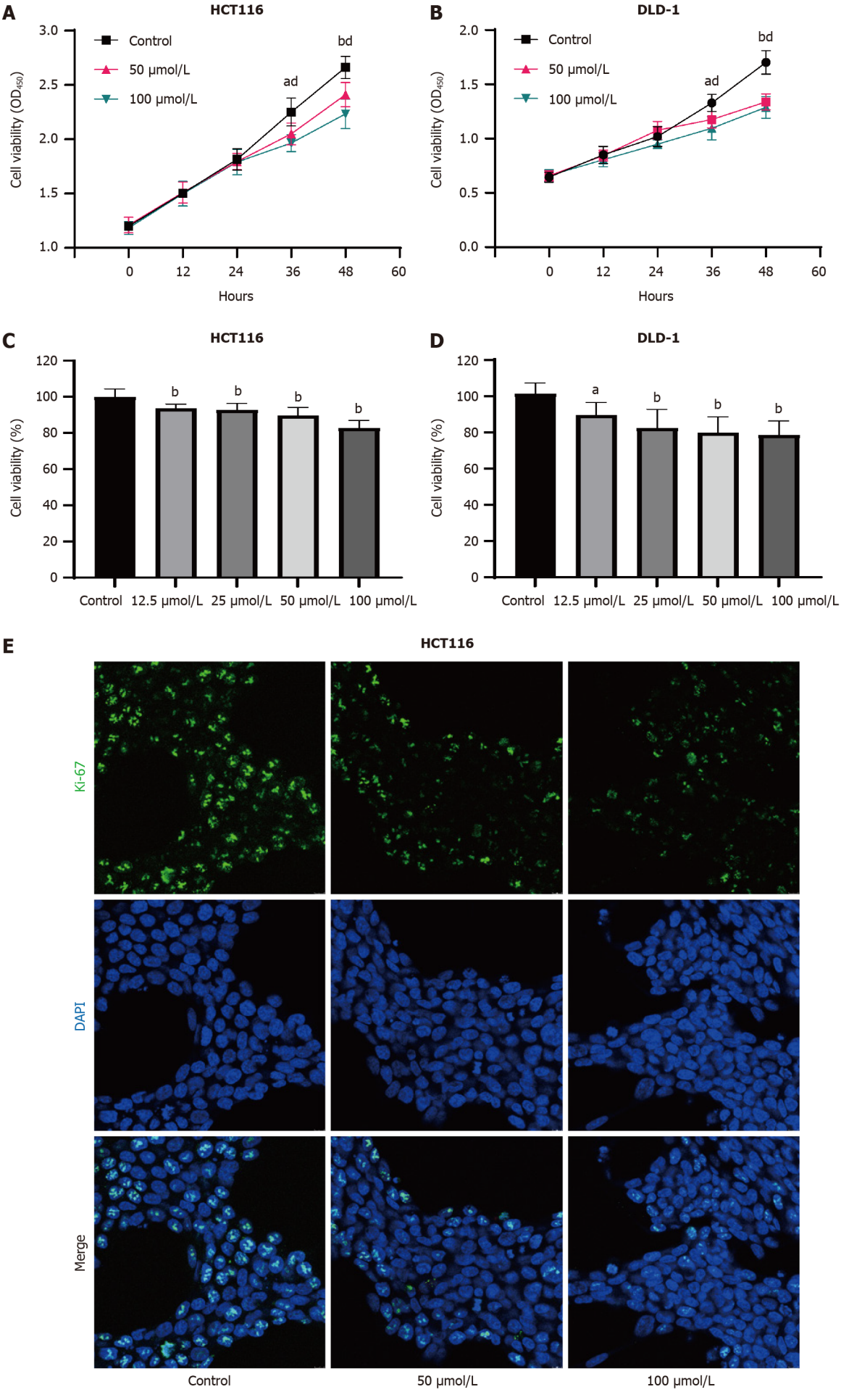
A
HCT116
Control
50 μmol/L
100 μmol/L
Cell viability (OD450)
Hours
ad
bd
B
DLD-1
C
HCT116
Cell viability (%)
Control
12.5 μmol/L
25 μmol/L
50 μmol/L
100 μmol/L
D
DLD-1
E
HCT116
Ki-67
DAPI
Merge
Control
50 μmol/L
100 μmol/L

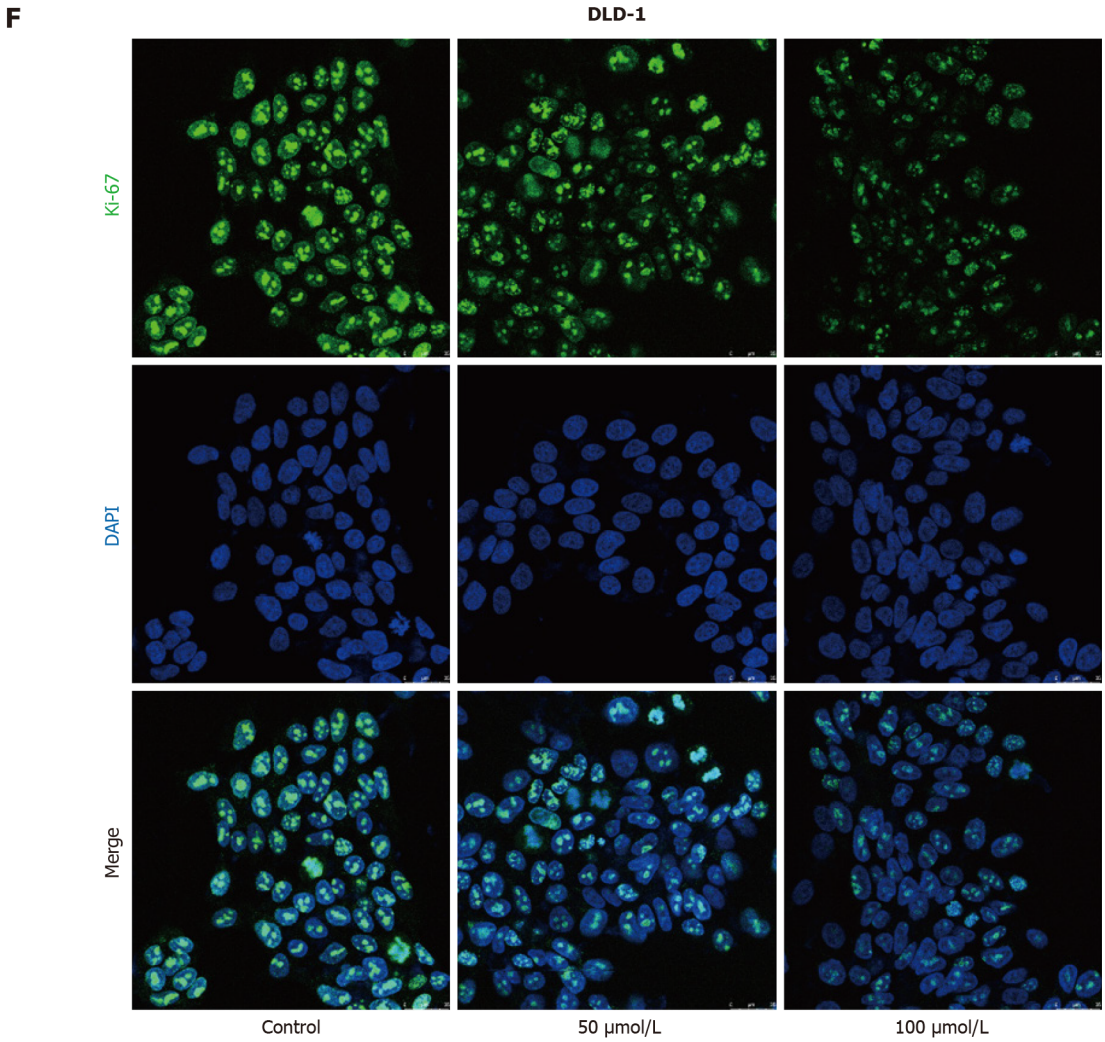

Figure 2 Indole-3-acetaldehyde inhibits proliferation of colorectal cancer cells *in vitro*. A and B: Growth curves of HCT116 and DLD-1 cells treated with IAAD; C and D: Vitality of HCT116 and DLD-1 cells treated with different concentrations of indole-3-acetaldehyde after 48 h, compared with the control group; E and F: The expression of Ki-67 in the nucleus was determined by immunofluorescence. $^{a}P < 0.05$, 50 μmol/L indole-3-acetaldehyde treatment group *vs* control group; $^{b}P < 0.01$, 50 μmol/L indole-3-acetaldehyde treatment group *vs* control group; $^{d}P < 0.01$, 100 μmol/L indole-3-acetaldehyde treatment group *vs* control group. DAPI: 4',6-diamidino-2-phenylindole.

tioned targets. The enrichment functions of these proteins were as follows: (1) Biological process: The cellular response to collagen catabolic process and response to xenobiotic stimulus in biological processes; (2) molecular function: Sodium symporter activity and cysteine-type peptidase activity; and (3) cellular component: Integral component of the plasma membrane and neuron projection region (Figure 6A). The genes associated with the top 20 pathways ($P < 0.05$) were associated with neuroactive ligand-receptor interactions, dopaminergic synapses, and alcoholism, among other factors (Figure 6B).

The PPI networks were analyzed using Cytoscape 3.9.1, and the cytoHubba and MCODE plug-ins were used to screen the core targets (Figure 6C-F). Seven core targets were identified, including matrix metalloproteinase-9 (MMP9), angiotensin converting enzyme (ACE), poly ADP-ribose polymerase-1 (PARP1), histone deacetylase-2, matrix metalloproteinase-2 (MMP2), myeloperoxidase (MPO), and nuclear receptor corepressor-1. Afterward, molecular docking of these targets and IAAD was performed. The results showed that IAAD could bind effectively to MMP9, ACE, PARP1, MMP2, and MPO *via* H-bonds, with a binding energy of less than -5.0 kJ/m^2 (Table 2 and Figure 7).

DISCUSSION

Although Trp is the least abundant amino acid in proteins and cells, it is an important biosynthetic precursor for a large number of microbial and host metabolites[23]. Trp can be further metabolized *via* three metabolic pathways: (1) The indole pathway[24]; (2) the kynurenine (Kyn) pathway[25]; and (3) the tryptamine pathway[26]. Approximately 90%-95% of Trp[27] is converted to Kyn and its downstream metabolites, including canavanine, 3-hydroxykynurine, and quinolinic acid. Many Kyn-related intermediate metabolites or enzymes are associated with the development of CRC[28-35]. Moreover, 4%-6% of unabsorbed Trp subsequently moves through the gastrointestinal tract and is metabolized by

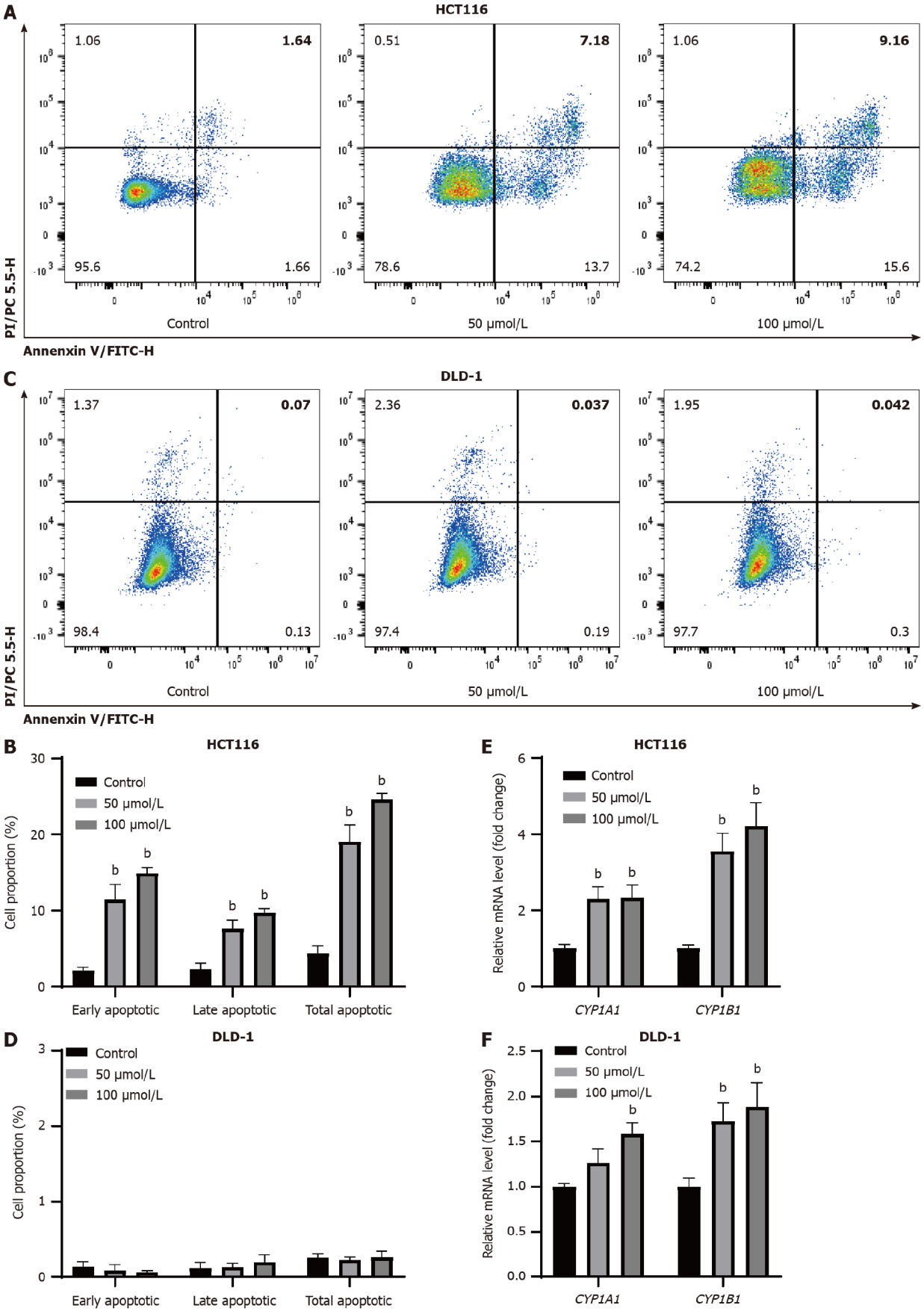

Figure 3 Indole-3-acetaldehyde induces apoptosis in HCT116 cells. A-D: Apoptosis of colorectal cancer cells was observed by annexin V-fluorescein isothiocyanate/propidium iodide co-staining; E and F: The relative mRNA levels of downstream genes regulated by aryl hydrocarbon receptor were determined by real-time fluorescence quantitative polymerase chain reaction. $^{b}P < 0.01$ *vs* control group. *CYP1A1*: Cytochrome P450 family 1 subfamily A member 1; *CYP1B1*: Cytochrome P450 family 1 subfamily B member 1.

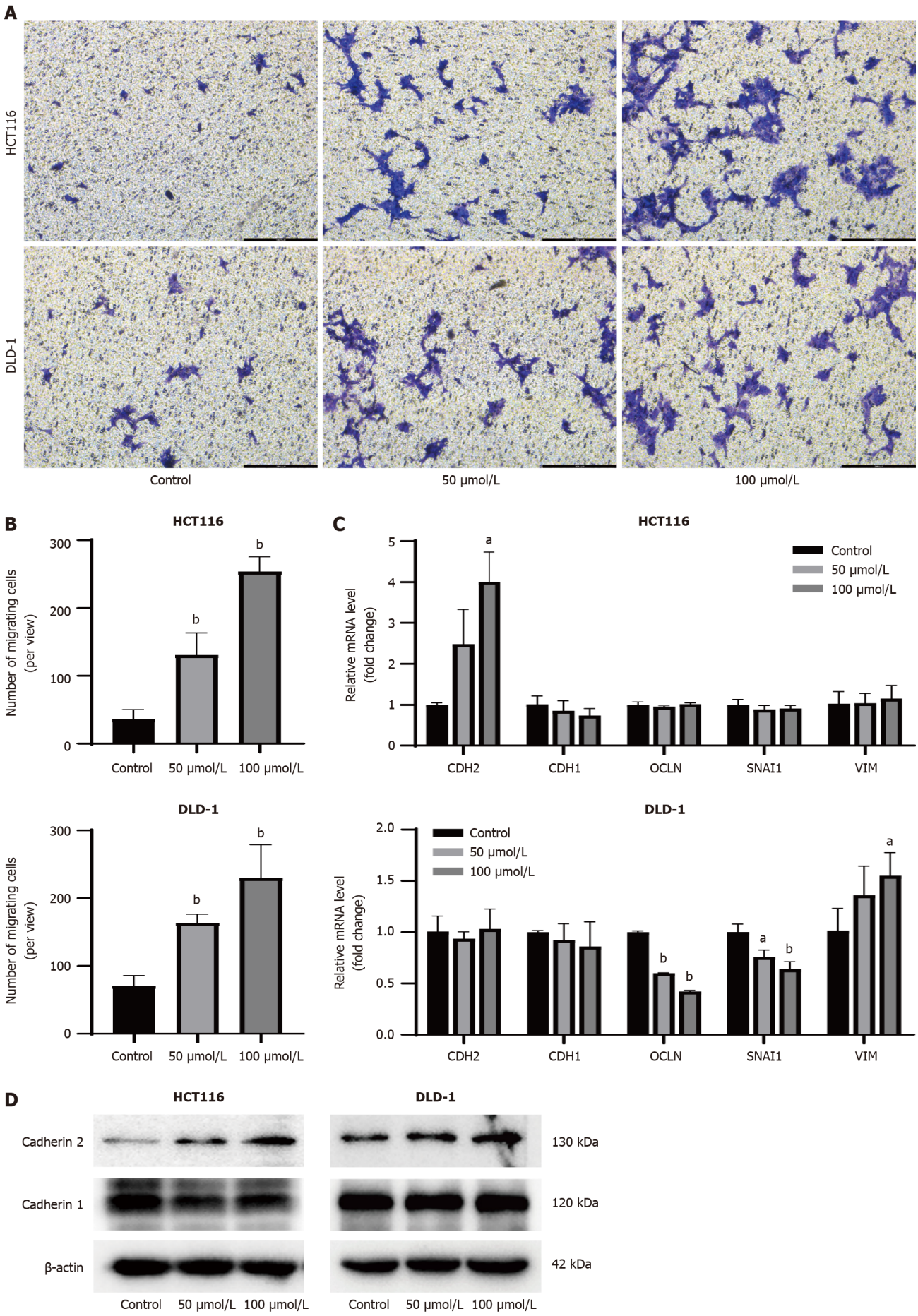
A
HCT116
DLD-1
Control
50 μmol/L
100 μmol/L
B
HCT116
Number of migrating cells (per view)
300
200
100
0
b
b
Control
50 μmol/L
100 μmol/L
C
HCT116
Relative mRNA level (fold change)
5
4
3
2
1
0
a
Control
50 μmol/L
100 μmol/L
CDH2
CDH1
OCLN
SNAI1
VIM
DLD-1
Number of migrating cells (per view)
300
200
100
0
b
b
Control
50 μmol/L
100 μmol/L
DLD-1
Relative mRNA level (fold change)
2.0
1.5
1.0
0.5
0.0
Control
50 μmol/L
100 μmol/L
b
b
a
b
a
CDH2
CDH1
OCLN
SNAI1
VIM
D
HCT116
DLD-1
Cadherin 2
Cadherin 1
β-actin
130 kDa
120 kDa
42 kDa
Control
50 μmol/L
100 μmol/L
Control
50 μmol/L
100 μmol/L

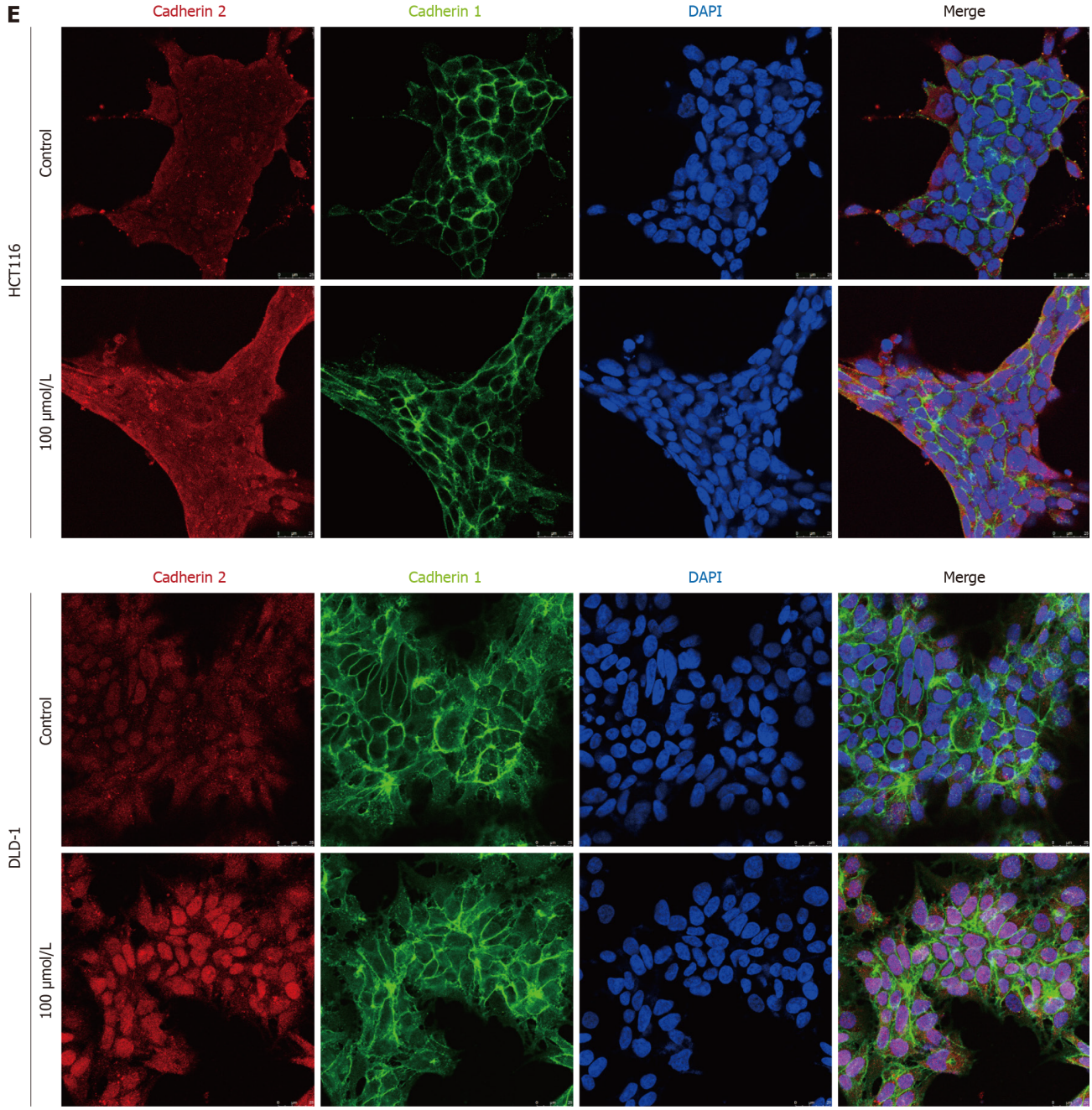

Figure 4 Indole-3-acetaldehyde promotes invasiveness and epithelial-mesenchymal transition of colorectal cancer cell lines. A: Crystal violet staining image of cells in the lower chamber (100 ×); B: Quantitative analysis of cell numbers in the lower chamber; C: Changes in the mRNA expression levels of cadherin 1, cadherin 2, occludin, snail family transcriptional repressor 1, and vimentin in the HCT116 and DLD-1 cells; D: Western blotting was used to detect the expression of intracellular cadherin; E: The expression and subcellular localization of cadherin were determined by immunofluorescence. $^{a}P < 0.05$ *vs* control group; $^{b}P < 0.01$ *vs* control group. DAPI: 4',6-diamidino-2-phenylindole; *CDH1*: Cadherin 1; *CDH2*: Cadherin 2; *OCLN*: Occludin; *SNAI1*: Snail family transcriptional repressor 1; *VIM*: Vimentin.

microorganisms into indoles and indole-like compounds[13]. Interestingly, indole levels are decreased in the intestines of patients with CRC, and several new studies have been conducted to elucidate how indole derivatives inhibit CRC[36,37]. *In vivo* and *in vitro* cellular experiments have clearly demonstrated that indole-3-carbaldehyde[38] and indolelactate dehydrogenase can inhibit the proliferation and invasion ability of tumor cells. In the present study, the tumor suppressive effect of IAAD was also preliminarily observed in a syngeneic mouse model of CRC. To exclude the possibility that IAAD was metabolized by the bacterial colony into other indole derivatives with tumor-suppressive functions in mice, further experiments based on CRC cell lines were performed. Cytotoxicity assays and Ki-67 immunofluorescence staining confirmed the direct inhibitory effect of IAAD on the proliferation of CRC tumor cells.

There are many mechanisms by which indole derivatives inhibit colon cancer, and apoptosis induction is one of the key mechanisms. For example, the anticancer mechanism of indole-3-methanol (IC) mainly involves the upregulation of the tumor suppressor protein p53 and the activation of apoptotic factors to induce the apoptosis of tumor cells[18,39]; moreover, the combination of dietary IC and Synthroid increases the transcription level of Raf1 and reduces tumor

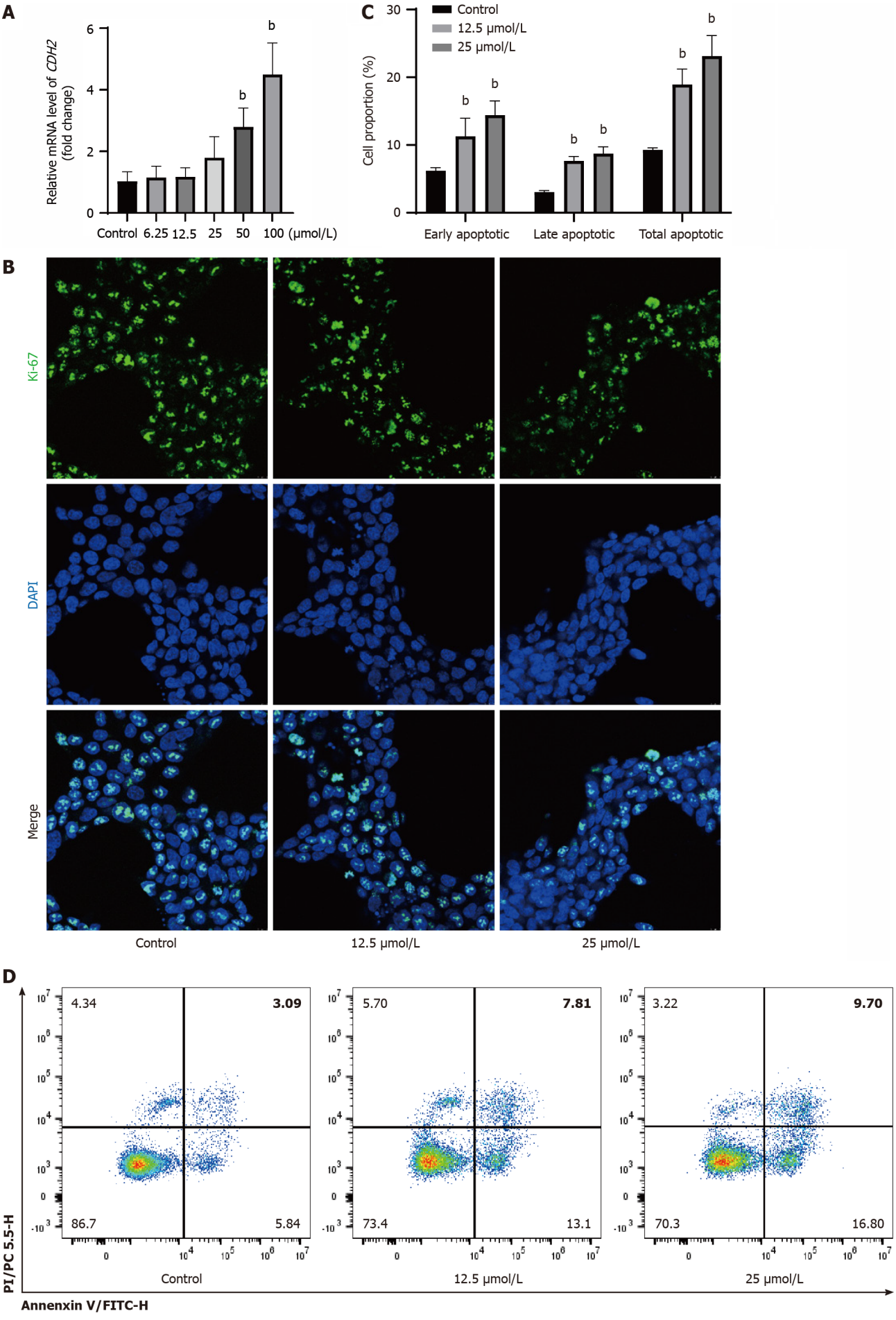
A
Relative mRNA level of CDH2 (fold change)
Control 6.25 12.5 25 50 100 (μmol/L)
C
Control
12.5 μmol/L
25 μmol/L
Cell proportion (%)
Early apoptotic
Late apoptotic
Total apoptotic
B
Ki-67
DAPI
Merge
Control
12.5 μmol/L
25 μmol/L
D
4.34
3.09
86.7
5.84
5.70
7.81
73.4
13.1
3.22
9.70
70.3
16.80
PI/PC 5.5-H
Annexin V/FITC-H
Control
12.5 μmol/L
25 μmol/L

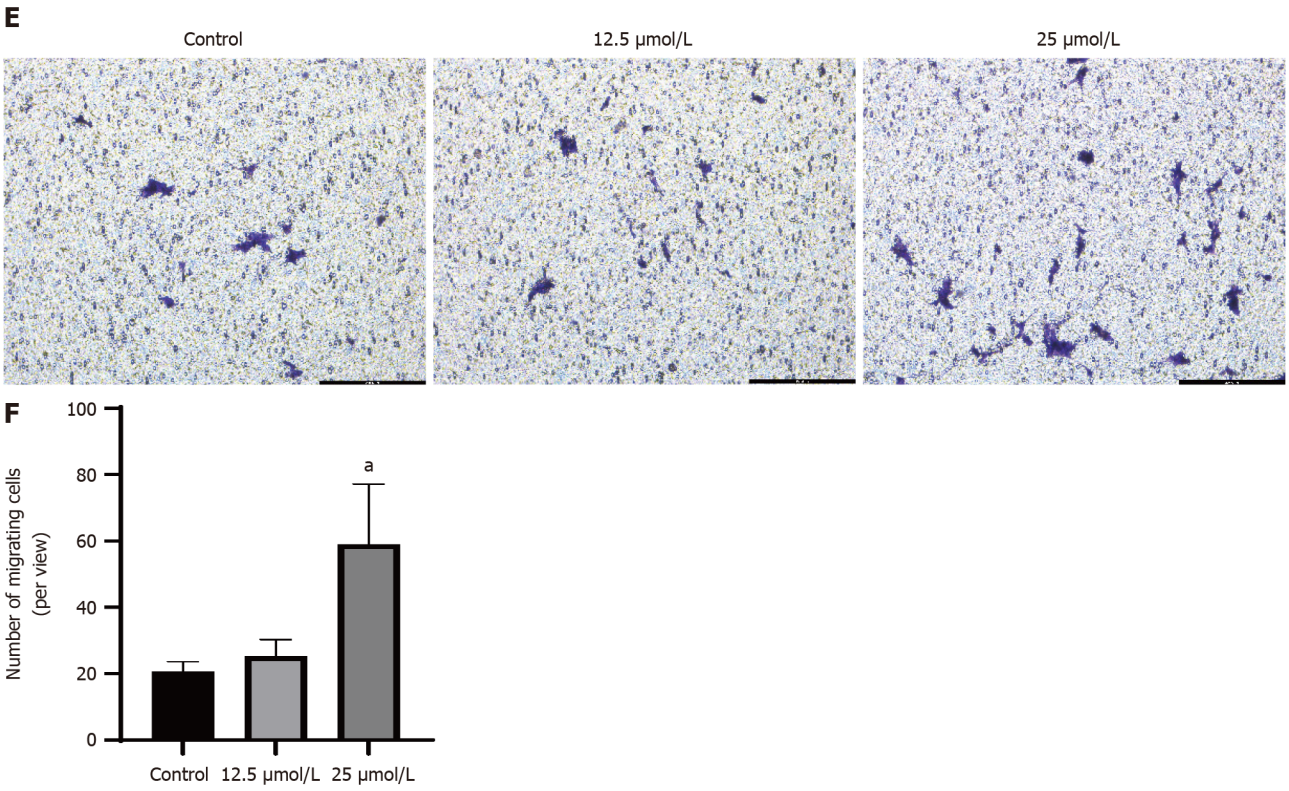

Figure 5 Indole-3-acetaldehyde at a concentration of 12.5 μmol/L is only cytotoxic and does not promote invasiveness. A: Relative mRNA expression levels of Cadherin 2 in HCT116 cells; B: The expression of Ki-67 in the nucleus was determined *via* immunofluorescence; C and D: Apoptosis of HCT116 cells was observed by annexin V-fluorescein isothiocyanate/propidium iodide co-staining E: Crystal violet staining image of HCT116 cells in the lower chamber (100 ×); F: Quantitative analysis of HCT116 cell numbers in the lower chamber. $^{a}P < 0.05$ *vs* control group; $^{b}P < 0.01$ *vs* control group. *CDH2*: Cadherin 2; DAPI: 4',6-diamidino-2-phenylindole.

progression and invasiveness associated with the *Cdh1* and *Appl1* genes[40]. ILA promotes apoptosis in human CRC cell lines (HCT-116 and LoVo) without affecting normal colonic epithelial cells[41]. Additionally, IAA inhibits CRC cell proliferation through the activation of TLR4-mediated JNK[42]. 3,3'-Diindolylmethane, which is the main condensation product of IC *in vivo*, can induce the apoptosis of human CRC cells by stimulating the expression of ATF3 through the ATF4-mediated pathway[43]. Another study screened the tumor-suppressive effects of 10 indole derivatives, among which the K-453 compound promoted apoptosis in CRC cell lines *in vitro* by downregulating the NF-κB1 (p50) and RelA (p65) proteins[44]. Additionally, synthetic isatin-indole couplings (7A-E and 9A-E) are also used as potential anticancer agents. Bcl-2 and Bcl-xL are inhibitors that induce apoptosis in tumor cells[45]. The present study also showed that IAAD increased the proportion of early and late apoptotic HCT116 cells but had no apoptosis-promoting effect on the DLD-1 cell line. Thus, there may be multiple pathways and mechanisms by which IAAD leads to programmed cell death in CRC cells.

The AhR can be activated by many indole derivatives, such as indole-3-aldehyde, indole-3-acid-acetic acid, indole-3-propionic acid, ILA, and IAAD[46,47], which are partly responsible for the induction of tumor cell apoptosis[48]. Studies have shown that in a colitis-related colorectal tumor mouse model, the number of colorectal tumors increased after AhR was knocked out[49]. Additionally, the cytotoxic and pro-apoptotic effects of I3C on CRC cells have been demonstrated *in vivo* and *in vitro*, and these therapeutic effects can be reversed by *AhR* gene inhibition[18,22]. In the present study, we examined AhR signaling activation in CRC cell lines and found that IAAD increased the mRNA abundance of two AhR target genes, *CYP1A1* and *CYP1B1*. These results suggested that IAAD, like other indole derivatives, may induce apoptosis in CRC cells by activating AhR. Notably, AhR activation in the HCT116 cell line was much greater than that in the DLD-1 cell line, which may explain why apoptosis can only be observed in HCT116 cells.

Subsequently, we observed the effect of IAAD on tumor cell invasiveness. Unexpectedly, the results of the transwell assay showed that IAAD promoted the invasiveness of HCT116 and DLD-1 cells, and the changes in mRNA expression levels of *VIM*, *SNAI1*, and *OCLN* genes along with changes in protein and mRNA expression levels of *CDH1* and *CDH2* genes indicated that IAAD promoted the EMT of tumor cells at concentrations of 50 μmol/L and 100 μmol/L. Further studies suggested that low concentrations of IAAD (≤ 12.5 μmol/L) no longer had the aforementioned effects but still exhibited cytotoxicity. These results indicate that the role of gut microbiota metabolites in CRC is complex and that simply increasing the abundance of one metabolite in the intestine may not have a good tumor prevention effect.

To further explore the possible downstream targets of IAAD, the PharmMapper, SEA, and SWISS public databases were used to search for molecular targets of proteins that may interact with IAAD. A total of 99 possible predicted targets were identified, and their functions were enriched in the following aspects: (1) Biological process: Collagen catabolic process and response to xenobiotic stimulus; (2) molecular function: Sodium symporter activity and cysteine-type

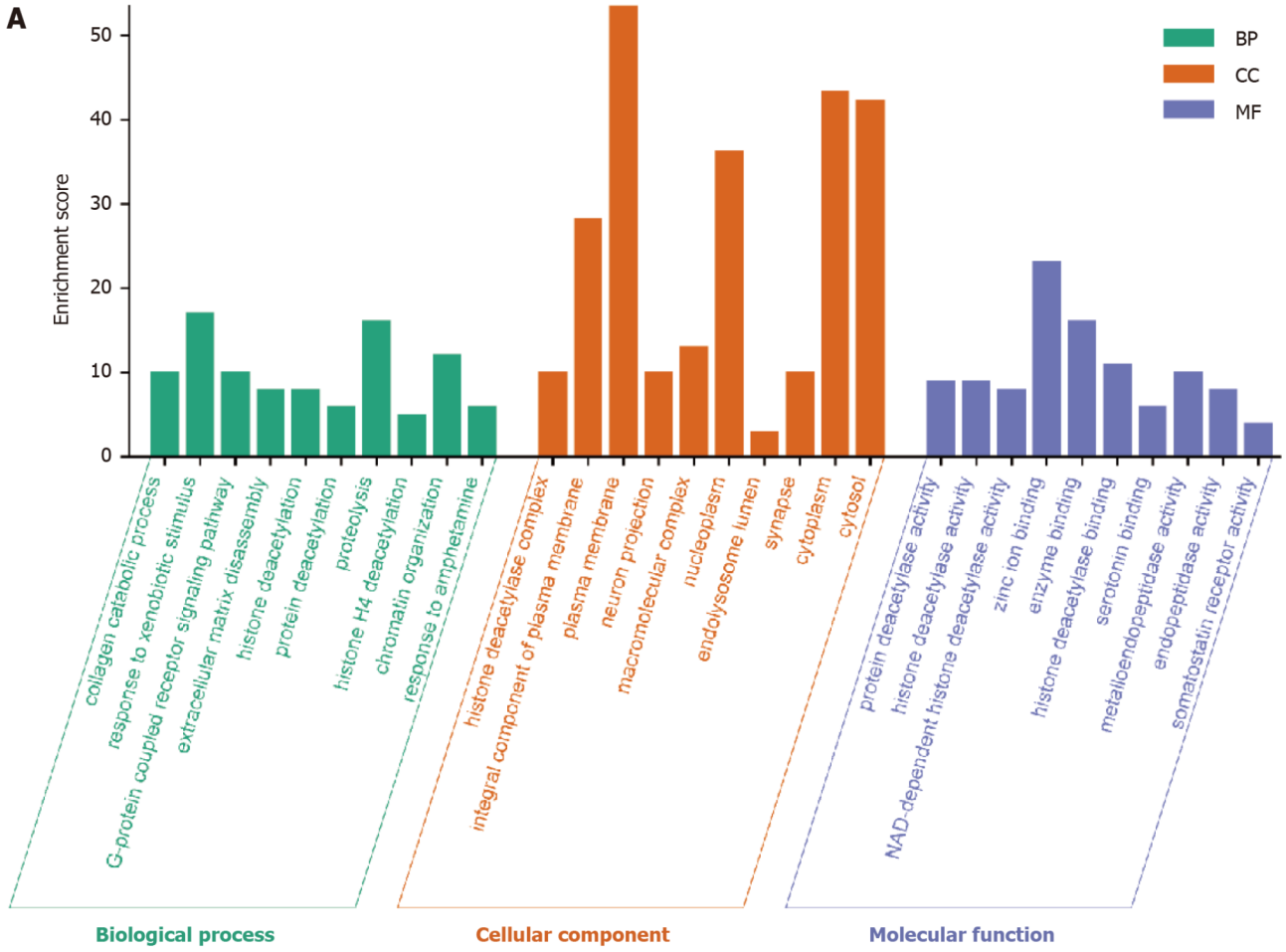
A
Enrichment score
0
10
20
30
40
50
BP
CC
MF
collagen catabolic process
response to xenobiotic stimulus
G-protein coupled receptor signaling pathway
extracellular matrix disassembly
histone deacetylation
protein deacetylation
proteolysis
histone H4 deacetylation
chromatin organization
response to amphetamine
histone deacetylase complex
integral component of plasma membrane
plasma membrane
neuron projection
macromolecular complex
nucleoplasm
endolysosome lumen
synapse
cytoplasm
cytosol
protein deacetylase activity
histone deacetylase activity
NAD-dependent histone deacetylase activity
zinc ion binding
enzyme binding
histone deacetylase binding
serotonin binding
metalloendopeptidase activity
endopeptidase activity
somatostatin receptor activity
Biological process
Cellular component
Molecular function

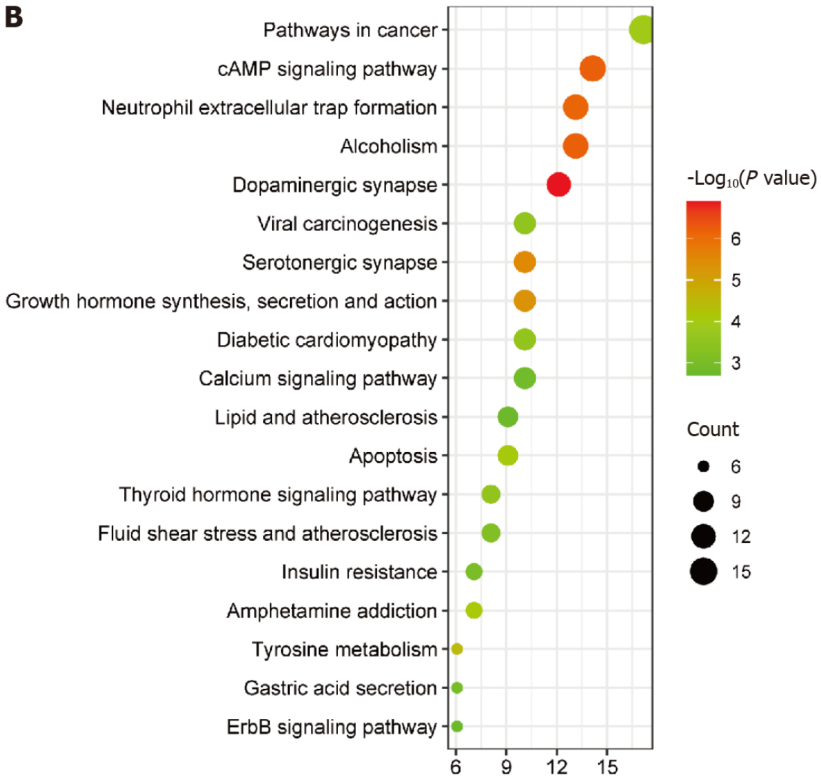
B
Pathways in cancer
cAMP signaling pathway
Neutrophil extracellular trap formation
Alcoholism
Dopaminergic synapse
Viral carcinogenesis
Serotonergic synapse
Growth hormone synthesis, secretion and action
Diabetic cardiomyopathy
Calcium signaling pathway
Lipid and atherosclerosis
Apoptosis
Thyroid hormone signaling pathway
Fluid shear stress and atherosclerosis
Insulin resistance
Amphetamine addiction
Tyrosine metabolism
Gastric acid secretion
ErbB signaling pathway
6
9
12
15
-Log10(P value)
6
5
4
3
Count
6
9
12
15

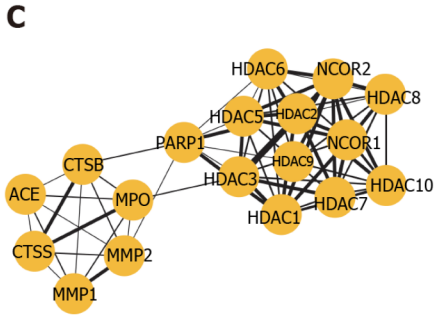
C
HDAC6
NCOR2
HDAC8
HDAC5
HDAC2
PARP1
NCOR1
CTSB
HDAC9
HDAC3
HDAC10
ACE
MPO
HDAC7
HDAC1
CTSS
MMP2
MMP1

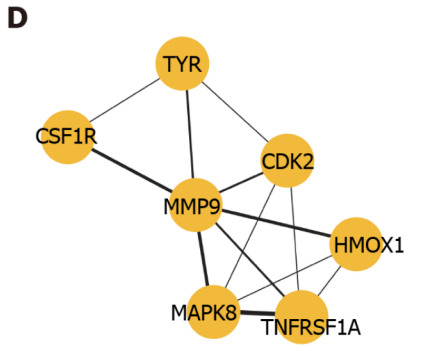
D
TYR
CSF1R
CDK2
MMP9
HMOX1
MAPK8
TNFRSF1A

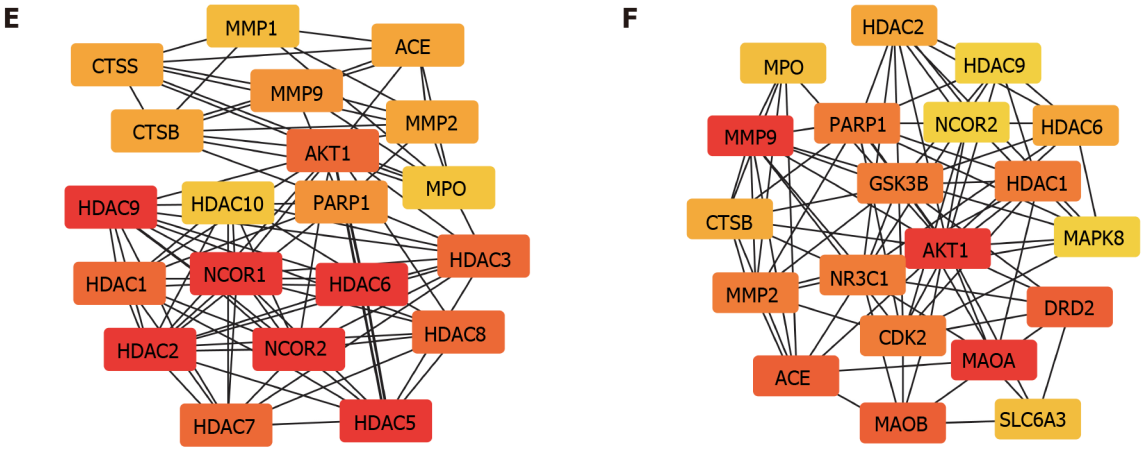

Figure 6 Target protein function prediction and core protein mining of indole-3-acetaldehyde. A: Analysis based on Gene Ontology database; B: Analysis based on Kyoto Encyclopedia of Genes and Genome database; C and D: Results of the cytoHubba plug-in analysis; E and F: Results of the MCODE plug-in analysis. ACE: Angiotensin converting enzyme; CTSB: Cathepsin B; MPO: Myeloperoxidase; MMP: Matrix Metallopeptidase; CTSS: Cathepsin S; PARP: Poly (ADP-Ribose) Polymerase; HDAC: Histone deacetylase; CSF1R: Colony stimulating factor 1 receptor; TYR: Tyrosinase; CDK: Cyclin dependent kinase; MAPK: Mitogen-activated protein kinase; HMOX: Heme oxygenase 1; TNFRSF1A: TNF receptor superfamily member 1A; NCOR: Nuclear receptor corepressor; GSK3B: Glycogen synthase kinase 3 beta; AKT: AKT serine/threonine kinase; NR3C1: Nuclear receptor subfamily 3 group c member 1; DRD2: Dopamine receptor D2; MAOA: Monoamine oxidase A; MAOB: Monoamine oxidase B; SLC6A3: Solute carrier family 6 member 3.

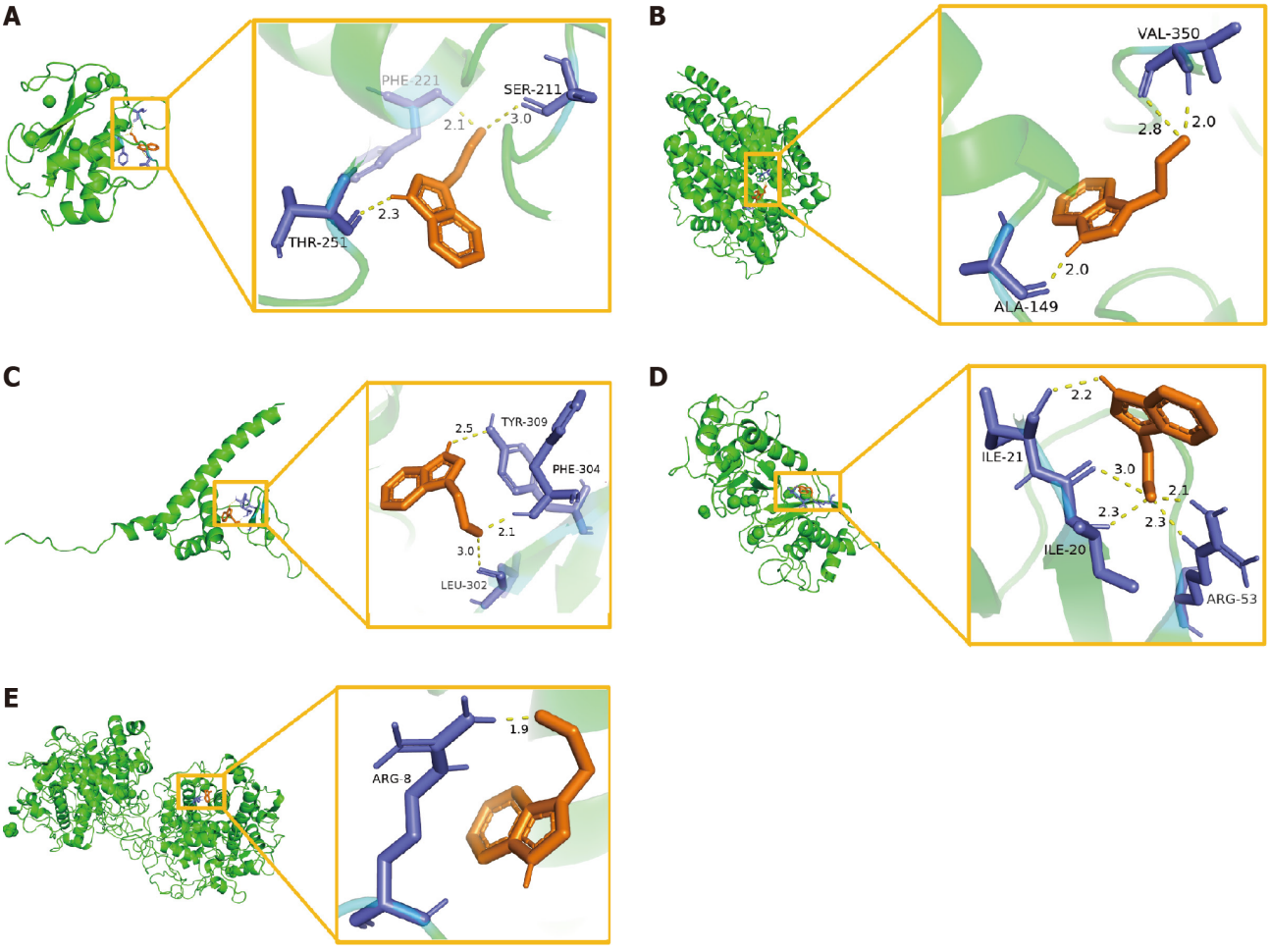

Figure 7 Molecular docking model of the predicted targets and indole-3-acetaldehyde. A: Matrix metalloproteinase-9-indole-3-acetaldehyde (IAAD); B: Angiotensin converting enzyme-IAAD; C: Poly ADP-ribose polymerase-1-IAAD; D: Matrix metalloproteinase-2-IAAD; E: Myeloperoxidase-IAAD. PHE: Phenylalanine; SER: Serine; THR: Threonine; VAL: Valine; ALA: Alanine; TYR: Tyrosine; LEU: Leucine; ILE: Isoleucine; ARG: Arginine.

Table 2 Dock details of target proteins and indole-3-acetaldehyde

Term	Binding energy (kcal/mol)	Mode of action	Target point (s)
6ESM-IAAD	-6.21	H bond	Phe221
1UZE-IAAD	-6.49	H bond	Ala149, Val350
2RIQ-IAAD	-5.52	H bond	Phe304
7XJO-IAAD	-5.62	H bond	ILE21, Arg53
4C1M-IAAD	-5.41	H bond	Arg8

IAAD: Indole-3-acetaldehyde; Phe: Phenylalanine; Val: Valine; Ala: Alanine; Ile: Isoleucine; Arg: Arginine; 6ESM: Identity marker of matrix metalloproteinase-9 protein crystal structures in Protein Data Bank databases (https://www.rcsb.org/); 1UZE: Angiotensin converting enzyme; 2RIQ: Poly ADP-ribose polymerase-1; 7XJO: Matrix metalloproteinase-2; 4C1M: Myeloperoxidase.

peptidase activity; and (3) cellular component: Integral component of the plasma membrane and neuron projection region. The core proteins, which included MMP2, MMP9, MPO, ACE, and PARP1, were identified *via* protein interaction analysis. IAAD can bind to Ile21 and Arg53 in MMP2, Phe221 in MMP9, Arg8 in MPO, Ala149 and Val350 in ACE, and Phe304 in PARP1 *via* hydrogen bonding. MMPs are reportedly associated with the metastasis of CRC. They can induce tumor angiogenesis and hydrolytically activate the transforming growth factor beta protein to promote EMT[50,51]. MMP2 and MMP9 are considered potential biomarkers of tumorigenesis, as are key effectors of EMT and important potential targets for antitumor therapies. Additionally, MPO is a major contributor to the development of multiple local inflammatory mediators of tissue damage in inflammatory diseases. Analysis of the The Cancer Genome Atlas cohort showed that MPO expression was upregulated in CRC tissues and significantly correlated with malignant progression in CRC patients[52]. Notably, activation of MPO can increase the expression of MMPs[53]. The binding of IAAD to the abovementioned proteins may be the key mechanism by which IAAD promotes invasive metastasis in CRC. However, additional *in vitro* experiments are needed to clarify this phenomenon.

CONCLUSION

In conclusion, the results of the present study demonstrate that the effect of IAAD on CRC is complex and bidirectional. At low concentrations (< 12.5 μmol/L), IAAD can inhibit tumor cell proliferation and induce tumor cell apoptosis. However, it induces both cytotoxicity and invasion at high concentrations (≥ 25 μmol/L). The numerous targets of IAAD may explain why it has a bidirectional effect. It can activate the AhR signaling pathway and directly interact with the key proteins MMP9, ACE, PARP1, MMP2, and MPO.

FOOTNOTES

Author contributions: Zhou YP designed and coordinated the study; Dai Z, Deng KL, and Wang XM performed the experiments, and acquired and analyzed the data; Dai Z and Tang CL interpreted the data; Dai Z, Wang XM, and Yang DX wrote the manuscript; all authors approved the final version of the article.

Supported by Zhejiang Provincial Natural Science Foundation of China, No. LTGD23C040008, No. LBY23H200006, and No. LQ22H030004.

Institutional review board statement: The study was reviewed and approved by the Ethics Committee of Ningbo University.

Institutional animal care and use committee statement: All procedures involving animals were reviewed and approved by the Institutional Animal Care and Use Committee of the Ningbo University Experimental Animal Center.

Conflict-of-interest statement: The authors declare that they have no conflict of interest to disclose.

Data sharing statement: No additional data are available.

ARRIVE guidelines statement: The authors have read the ARRIVE guidelines, and the manuscript was prepared and revised according to the ARRIVE guidelines.

Country/Territory of origin: China

ORCID number: Yu-Ping Zhou 0000-0001-8663-2153.

S-Editor: Qu XL
L-Editor: Wang TQ
P-Editor: Yuan YY

REFERENCES

1 **Sung H**, Ferlay J, Siegel RL, Laversanne M, Soerjomataram I, Jemal A, Bray F. Global Cancer Statistics 2020: GLOBOCAN Estimates of Incidence and Mortality Worldwide for 36 Cancers in 185 Countries. *CA Cancer J Clin* 2021; **71**: 209-249 [PMID: 33538338 DOI: 10.3322/caac.21660]
2 **Siegel RL**, Wagle NS, Cercek A, Smith RA, Jemal A. Colorectal cancer statistics, 2023. *CA Cancer J Clin* 2023; **73**: 233-254 [PMID: 36856579 DOI: 10.3322/caac.21772]
3 **Dekker E**, Tanis PJ, Vleugels JLA, Kasi PM, Wallace MB. Colorectal cancer. *Lancet* 2019; **394**: 1467-1480 [PMID: 31631858 DOI: 10.1016/S0140-6736(19)32319-0]
4 **Wong CC**, Yu J. Gut microbiota in colorectal cancer development and therapy. *Nat Rev Clin Oncol* 2023; **20**: 429-452 [PMID: 37169888 DOI: 10.1038/s41571-023-00766-x]
5 **Castellarin M**, Warren RL, Freeman JD, Dreolini L, Krzywinski M, Strauss J, Barnes R, Watson P, Allen-Vercoe E, Moore RA, Holt RA. Fusobacterium nucleatum infection is prevalent in human colorectal carcinoma. *Genome Res* 2012; **22**: 299-306 [PMID: 22009989 DOI: 10.1101/gr.126516.111]
6 **Feng Q**, Liang S, Jia H, Stadlmayr A, Tang L, Lan Z, Zhang D, Xia H, Xu X, Jie Z, Su L, Li X, Li J, Xiao L, Huber-Schönauer U, Niederseer D, Al-Aama JY, Yang H, Wang J, Kristiansen K, Arumugam M, Tilg H, Datz C. Gut microbiome development along the colorectal adenoma-carcinoma sequence. *Nat Commun* 2015; **6**: 6528 [PMID: 25758642 DOI: 10.1038/ncomms7528]
7 **Yu J**, Feng Q, Wong SH, Zhang D, Liang QY, Qin Y, Tang L, Zhao H, Stenvang J, Li Y, Wang X, Xu X, Chen N, Wu WK, Al-Aama J, Nielsen HJ, Kiilerich P, Jensen BA, Yau TO, Lan Z, Jia H, Li J, Xiao L, Lam TY, Ng SC, Cheng AS, Wong VW, Chan FK, Yang H, Madsen L, Datz C, Tilg H, Wang J, Brünner N, Kristiansen K, Arumugam M, Sung JJ. Metagenomic analysis of faecal microbiome as a tool towards targeted non-invasive biomarkers for colorectal cancer. *Gut* 2017; **66**: 70-78 [PMID: 26408641 DOI: 10.1136/gutjnl-2015-309800]
8 **Chang PV**, Hao L, Offermanns S, Medzhitov R. The microbial metabolite butyrate regulates intestinal macrophage function *via* histone deacetylase inhibition. *Proc Natl Acad Sci U S A* 2014; **111**: 2247-2252 [PMID: 24390544 DOI: 10.1073/pnas.1322269111]
9 **Buda A**, Qualtrough D, Jepson MA, Martines D, Paraskeva C, Pignatelli M. Butyrate downregulates alpha2beta1 integrin: a possible role in the induction of apoptosis in colorectal cancer cell lines. *Gut* 2003; **52**: 729-734 [PMID: 12692060 DOI: 10.1136/gut.52.5.729]
10 **Furusawa Y**, Obata Y, Fukuda S, Endo TA, Nakato G, Takahashi D, Nakanishi Y, Uetake C, Kato K, Kato T, Takahashi M, Fukuda NN, Murakami S, Miyauchi E, Hino S, Atarashi K, Onawa S, Fujimura Y, Lockett T, Clarke JM, Topping DL, Tomita M, Hori S, Ohara O, Morita T, Koseki H, Kikuchi J, Honda K, Hase K, Ohno H. Commensal microbe-derived butyrate induces the differentiation of colonic regulatory T cells. *Nature* 2013; **504**: 446-450 [PMID: 24226770 DOI: 10.1038/nature12721]
11 **Bernstein H**, Bernstein C, Payne CM, Dvorak K. Bile acids as endogenous etiologic agents in gastrointestinal cancer. *World J Gastroenterol* 2009; **15**: 3329-3340 [PMID: 19610133 DOI: 10.3748/wjg.15.3329]
12 **Bernstein C**, Holubec H, Bhattacharyya AK, Nguyen H, Payne CM, Zaitlin B, Bernstein H. Carcinogenicity of deoxycholate, a secondary bile acid. *Arch Toxicol* 2011; **85**: 863-871 [PMID: 21267546 DOI: 10.1007/s00204-011-0648-7]
13 **Wyatt M**, Greathouse KL. Targeting Dietary and Microbial Tryptophan-Indole Metabolism as Therapeutic Approaches to Colon Cancer. *Nutrients* 2021; **13** [PMID: 33916690 DOI: 10.3390/nu13041189]
14 **Li X**, Zhang B, Hu Y, Zhao Y. New Insights Into Gut-Bacteria-Derived Indole and Its Derivatives in Intestinal and Liver Diseases. *Front Pharmacol* 2021; **12**: 769501 [PMID: 34966278 DOI: 10.3389/fphar.2021.769501]
15 **Russell WR**, Duncan SH, Scobbie L, Duncan G, Cantlay L, Calder AG, Anderson SE, Flint HJ. Major phenylpropanoid-derived metabolites in the human gut can arise from microbial fermentation of protein. *Mol Nutr Food Res* 2013; **57**: 523-535 [PMID: 23349065 DOI: 10.1002/mnfr.201200594]
16 **Fong W**, Li Q, Ji F, Liang W, Lau HCH, Kang X, Liu W, To KK, Zuo Z, Li X, Zhang X, Sung JJ, Yu J. Lactobacillus gallinarum-derived metabolites boost anti-PD1 efficacy in colorectal cancer by inhibiting regulatory T cells through modulating IDO1/Kyn/AHR axis. *Gut* 2023; **72**: 2272-2285 [PMID: 37770127 DOI: 10.1136/gutjnl-2023-329543]
17 **Kurata K**, Ishii K, Koto Y, Naito K, Yuasa K, Shimizu H. Skatole-induced p38 and JNK activation coordinately upregulates, whereas AhR activation partially attenuates TNFα expression in intestinal epithelial cells. *Biosci Biotechnol Biochem* 2023; **87**: 611-619 [PMID: 36941128 DOI: 10.1093/bbb/zbad030]
18 **Megna BW**, Carney PR, Nukaya M, Geiger P, Kennedy GD. Indole-3-carbinol induces tumor cell death: function follows form. *J Surg Res* 2016; **204**: 47-54 [PMID: 27451867 DOI: 10.1016/j.jss.2016.04.021]
19 **Han JX**, Tao ZH, Wang JL, Zhang L, Yu CY, Kang ZR, Xie Y, Li J, Lu S, Cui Y, Xu J, Zhao E, Wang M, Chen J, Wang Z, Liu Q, Chen HM, Su W, Zou TH, Zhou CB, Hong J, Chen H, Xiong H, Chen YX, Fang JY. Microbiota-derived tryptophan catabolites mediate the chemopreventive effects of statins on colorectal cancer. *Nat Microbiol* 2023; **8**: 919-933 [PMID: 37069401 DOI: 10.1038/s41564-023-01363-5]
20 **Zhang Q**, Zhao Q, Li T, Lu L, Wang F, Zhang H, Liu Z, Ma H, Zhu Q, Wang J, Zhang X, Pei Y, Liu Q, Xu Y, Qie J, Luan X, Hu Z, Liu X. Lactobacillus plantarum-derived indole-3-lactic acid ameliorates colorectal tumorigenesis *via* epigenetic regulation of CD8(+) T cell immunity. *Cell Metab* 2023; **35**: 943-960.e9 [PMID: 37192617 DOI: 10.1016/j.cmet.2023.04.015]
21 **Plate AY**, Gallaher DD. Effects of indole-3-carbinol and phenethyl isothiocyanate on colon carcinogenesis induced by azoxymethane in rats. *Carcinogenesis* 2006; **27**: 287-292 [PMID: 16113056 DOI: 10.1093/carcin/bgi210]
22 **Lamouille S**, Xu J, Derynck R. Molecular mechanisms of epithelial-mesenchymal transition. *Nat Rev Mol Cell Biol* 2014; **15**: 178-196 [PMID:

24556840 DOI: 10.1038/nrm3758]
23 **Alkhalaf LM**, Ryan KS. Biosynthetic manipulation of tryptophan in bacteria: pathways and mechanisms. *Chem Biol* 2015; **22**: 317-328 [PMID: 25794436 DOI: 10.1016/j.chembiol.2015.02.005]
24 **Zelante T**, Iannitti RG, Cunha C, De Luca A, Giovannini G, Pieraccini G, Zecchi R, D'Angelo C, Massi-Benedetti C, Fallarino F, Carvalho A, Puccetti P, Romani L. Tryptophan catabolites from microbiota engage aryl hydrocarbon receptor and balance mucosal reactivity *via* interleukin-22. *Immunity* 2013; **39**: 372-385 [PMID: 23973224 DOI: 10.1016/j.immuni.2013.08.003]
25 **Clarke G**, McKernan DP, Gaszner G, Quigley EM, Cryan JF, Dinan TG. A Distinct Profile of Tryptophan Metabolism along the Kynurenine Pathway Downstream of Toll-Like Receptor Activation in Irritable Bowel Syndrome. *Front Pharmacol* 2012; **3**: 90 [PMID: 22661947 DOI: 10.3389/fphar.2012.00090]
26 **Yano JM**, Yu K, Donaldson GP, Shastri GG, Ann P, Ma L, Nagler CR, Ismagilov RF, Mazmanian SK, Hsiao EY. Indigenous bacteria from the gut microbiota regulate host serotonin biosynthesis. *Cell* 2015; **161**: 264-276 [PMID: 25860609 DOI: 10.1016/j.cell.2015.02.047]
27 **Dehhaghi M**, Kazemi Shariat Panahi H, Guillemin GJ. Microorganisms, Tryptophan Metabolism, and Kynurenine Pathway: A Complex Interconnected Loop Influencing Human Health Status. *Int J Tryptophan Res* 2019; **12**: 1178646919852996 [PMID: 31258331 DOI: 10.1177/1178646919852996]
28 **Tevini J**, Eder SK, Huber-Schönauer U, Niederseer D, Strebinger G, Gostner JM, Aigner E, Datz C, Felder TK. Changing Metabolic Patterns along the Colorectal Adenoma-Carcinoma Sequence. *J Clin Med* 2022; **11** [PMID: 35160173 DOI: 10.3390/jcm11030721]
29 **Engin AB**, Karahalil B, Karakaya AE, Engin A. Helicobacter pylori and serum kynurenine-tryptophan ratio in patients with colorectal cancer. *World J Gastroenterol* 2015; **21**: 3636-3643 [PMID: 25834331 DOI: 10.3748/wjg.v21.i12.3636]
30 **Crotti S**, D'angelo E, Bedin C, Fassan M, Pucciarelli S, Nitti D, Bertazzo A, Agostini M. Tryptophan metabolism along the kynurenine and serotonin pathways reveals substantial differences in colon and rectal cancer. *Metabolomics* 2017; **13**: 148 [DOI: 10.1007/s11306-017-1288-6]
31 **Liu CY**, Huang TT, Chen JL, Chu PY, Lee CH, Lee HC, Lee YH, Chang YY, Yang SH, Jiang JK, Chen WS, Chao Y, Teng HW. Significance of Kynurenine 3-Monooxygenase Expression in Colorectal Cancer. *Front Oncol* 2021; **11**: 620361 [PMID: 33937026 DOI: 10.3389/fonc.2021.620361]
32 **Singh SK**, Banerjee S, Acosta EP, Lillard JW, Singh R. Resveratrol induces cell cycle arrest and apoptosis with docetaxel in prostate cancer cells *via* a p53/ p21WAF1/CIP1 and p27KIP1 pathway. *Oncotarget* 2017; **8**: 17216-17228 [PMID: 28212547 DOI: 10.18632/oncotarget.15303]
33 **Wu D**, Zhu Y. Role of kynurenine in promoting the generation of exhausted CD8(+) T cells in colorectal cancer. *Am J Transl Res* 2021; **13**: 1535-1547 [PMID: 33841677]
34 **Campia I**, Buondonno I, Castella B, Rolando B, Kopecka J, Gazzano E, Ghigo D, Riganti C. An Autocrine Cytokine/JAK/STAT-Signaling Induces Kynurenine Synthesis in Multidrug Resistant Human Cancer Cells. *PLoS One* 2015; **10**: e0126159 [PMID: 25955018 DOI: 10.1371/journal.pone.0126159]
35 **Liu M**, Wang X, Wang L, Ma X, Gong Z, Zhang S, Li Y. Targeting the IDO1 pathway in cancer: from bench to bedside. *J Hematol Oncol* 2018; **11**: 100 [PMID: 30068361 DOI: 10.1186/s13045-018-0644-y]
36 **Ferdinande L**, Decaestecker C, Verset L, Mathieu A, Moles Lopez X, Negulescu AM, Van Maerken T, Salmon I, Cuvelier CA, Demetter P. Clinicopathological significance of indoleamine 2,3-dioxygenase 1 expression in colorectal cancer. *Br J Cancer* 2012; **106**: 141-147 [PMID: 22108515 DOI: 10.1038/bjc.2011.513]
37 **Murphy AG**, Zheng L. Small molecule drugs with immunomodulatory effects in cancer. *Hum Vaccin Immunother* 2015; **11**: 2463-2468 [PMID: 26110550 DOI: 10.1080/21645515.2015.1057363]
38 **McGrath DR**, Spigelman AD. Putative mechanisms of action for indole-3-carbinol in the prevention of colorectal cancer. *Expert Opin Ther Targets* 2008; **12**: 729-738 [PMID: 18479219 DOI: 10.1517/14728222.12.6.729]
39 **Lee JY**, Lim HM, Lee CM, Park SH, Nam MJ. Indole-3-carbinol inhibits the proliferation of colorectal carcinoma LoVo cells through activation of the apoptotic signaling pathway. *Hum Exp Toxicol* 2021; **40**: 2099-2112 [PMID: 34085558 DOI: 10.1177/09603271211021475]
40 **de Moura NA**, Caetano BFR, de Moraes LN, Carvalho RF, Rodrigues MAM, Barbisan LF. Enhancement of colon carcinogenesis by the combination of indole-3 carbinol and synbiotics in hemin-fed rats. *Food Chem Toxicol* 2018; **112**: 11-18 [PMID: 29269057 DOI: 10.1016/j.fct.2017.12.029]
41 **Sugimura N**, Li Q, Chu ESH, Lau HCH, Fong W, Liu W, Liang C, Nakatsu G, Su ACY, Coker OO, Wu WKK, Chan FKL, Yu J. Lactobacillus gallinarum modulates the gut microbiota and produces anti-cancer metabolites to protect against colorectal tumourigenesis. *Gut* 2021; **71**: 2011-2021 [PMID: 34937766 DOI: 10.1136/gutjnl-2020-323951]
42 **Tomii A**, Higa M, Naito K, Kurata K, Kobayashi J, Takei C, Yuasa K, Koto Y, Shimizu H. Activation of the TLR4-JNK but not the TLR4-ERK pathway induced by indole-3-acetic acid exerts anti-proliferative effects on Caco-2 cells. *Biosci Biotechnol Biochem* 2023; **87**: 839-849 [PMID: 37147026 DOI: 10.1093/bbb/zbad055]
43 **Lee SH**, Min KW, Zhang X, Baek SJ. 3,3'-diindolylmethane induces activating transcription factor 3 (ATF3) *via* ATF4 in human colorectal cancer cells. *J Nutr Biochem* 2013; **24**: 664-671 [PMID: 22819556 DOI: 10.1016/j.jnutbio.2012.03.016]
44 **Tischlerova V**, Kello M, Budovska M, Mojzis J. Indole phytoalexin derivatives induce mitochondrial-mediated apoptosis in human colorectal carcinoma cells. *World J Gastroenterol* 2017; **23**: 4341-4353 [PMID: 28706417 DOI: 10.3748/wjg.v23.i24.4341]
45 **Eldehna WM**, Abo-Ashour MF, Al-Warhi T, Al-Rashood ST, Alharbi A, Ayyad RR, Al-Khayal K, Abdulla M, Abdel-Aziz HA, Ahmad R, El-Haggar R. Development of 2-oindolin-3-ylidene-indole-3-carbohydrazide derivatives as novel apoptotic and anti-proliferative agents towards colorectal cancer cells. *J Enzyme Inhib Med Chem* 2021; **36**: 319-328 [PMID: 33345633 DOI: 10.1080/14756366.2020.1862100]
46 **Alexeev EE**, Lanis JM, Kao DJ, Campbell EL, Kelly CJ, Battista KD, Gerich ME, Jenkins BR, Walk ST, Kominsky DJ, Colgan SP. Microbiota-Derived Indole Metabolites Promote Human and Murine Intestinal Homeostasis through Regulation of Interleukin-10 Receptor. *Am J Pathol* 2018; **188**: 1183-1194 [PMID: 29454749 DOI: 10.1016/j.ajpath.2018.01.011]
47 **Hubbard TD**, Murray IA, Perdew GH. Indole and Tryptophan Metabolism: Endogenous and Dietary Routes to Ah Receptor Activation. *Drug Metab Dispos* 2015; **43**: 1522-1535 [PMID: 26041783 DOI: 10.1124/dmd.115.064246]
48 **Ronnekleiv-Kelly SM**, Nukaya M, Díaz-Díaz CJ, Megna BW, Carney PR, Geiger PG, Kennedy GD. Aryl hydrocarbon receptor-dependent apoptotic cell death induced by the flavonoid chrysin in human colorectal cancer cells. *Cancer Lett* 2016; **370**: 91-99 [PMID: 26515162 DOI: 10.1016/j.canlet.2015.10.014]
49 **Díaz-Díaz CJ**, Ronnekleiv-Kelly SM, Nukaya M, Geiger PG, Balbo S, Dator R, Megna BW, Carney PR, Bradfield CA, Kennedy GD. The Aryl Hydrocarbon Receptor is a Repressor of Inflammation-associated Colorectal Tumorigenesis in Mouse. *Ann Surg* 2016; **264**: 429-436 [PMID: 27433903 DOI: 10.1097/SLA.0000000000001874]

50 **Coussens LM**, Fingleton B, Matrisian LM. Matrix metalloproteinase inhibitors and cancer: trials and tribulations. *Science* 2002; **295**: 2387-2392 [PMID: 11923519 DOI: 10.1126/science.1067100]

51 **Ara T**, Fukuzawa M, Kusafuka T, Komoto Y, Oue T, Inoue M, Okada A. Immunohistochemical expression of MMP-2, MMP-9, and TIMP-2 in neuroblastoma: association with tumor progression and clinical outcome. *J Pediatr Surg* 1998; **33**: 1272-1278 [PMID: 9722003 DOI: 10.1016/s0022-3468(98)90167-1]

52 **Weng M**, Yue Y, Wu D, Zhou C, Guo M, Sun C, Liao Q, Sun M, Zhou D, Miao C. Increased MPO in Colorectal Cancer Is Associated With High Peripheral Neutrophil Counts and a Poor Prognosis: A TCGA With Propensity Score-Matched Analysis. *Front Oncol* 2022; **12**: 940706 [PMID: 35912260 DOI: 10.3389/fonc.2022.940706]

53 **Peltonen R**, Hagström J, Tervahartiala T, Sorsa T, Haglund C, Isoniemi H. High Expression of MMP-9 in Primary Tumors and High Preoperative MPO in Serum Predict Improved Prognosis in Colorectal Cancer with Operable Liver Metastases. *Oncology* 2021; **99**: 144-160 [PMID: 33027796 DOI: 10.1159/000510609]

Published by **Baishideng Publishing Group Inc**
7041 Koll Center Parkway, Suite 160, Pleasanton, CA 94566, USA
Telephone: +1-925-3991568
E-mail: office@baishideng.com
Help Desk: https://www.f6publishing.com/helpdesk
https://www.wjgnet.com